Swift follow-up of unidentified X-ray sources in the *XMM–Newton* Slew Survey

R. L. C. Starling,[1]★ P. A. Evans,[1] A. M. Read,[1] R. D. Saxton,[2] P. Esquej,[1] H. Krimm,[3,4] P. T. O'Brien,[1] J. P. Osborne,[1] S. Mateos,[1] R. Warwick[1] and K. Wiersema[1]

[1]*Department of Physics and Astronomy, University of Leicester, University Road, Leicester LE1 7RH*
[2]*XMM–Newton SOC, ESAC, Apartado 78, 28691 Villanueva de la Cañada, Madrid, Spain*
[3]*Universities Space Research Association, Columbia, MD 20144, USA*
[4]*NASA/Goddard Space Flight Center, Greenbelt, MD 20771, USA*

ABSTRACT

We present deep *Swift* follow-up observations of a sample of 94 unidentified X-ray sources from the *XMM–Newton* Slew Survey. The X-ray Telescope (XRT) on-board *Swift* detected 29 per cent of the sample sources; the flux limits for undetected sources suggest the bulk of the Slew Survey sources are drawn from one or more transient populations. We report revised X-ray positions for the XRT-detected sources, with typical uncertainties of 2.9 arcsec, reducing the number of catalogued optical matches to just a single source in most cases. We characterize the sources detected by *Swift* through their X-ray spectra and variability and via Ultraviolet–Optical Telescope photometry and using catalogued near-infrared, optical and radio observations of potential counterparts. Six sources can be associated with known objects and eight sources may be associated with unidentified *ROSAT* sources within the 3σ error radii of our revised X-ray positions. We find 10 of the 30 XRT- and/or Burst Alert Telescope (BAT)-detected sources are clearly stellar in nature, including one periodic variable star and two high proper motion stars. For 11 sources we propose an active galactic nucleus (AGN) classification, among which four are detected in hard X-rays and three have redshifts spanning $z = 0.2$–0.9 obtained from the literature or from optical spectroscopy presented here. A further three sources are suspected AGN and one is a candidate Galactic hard X-ray flash, while five sources remain unclassified. The 67 Slew Survey sources we do not detect with *Swift* XRT or BAT are studied via their characteristics in the Slew Survey observations and by comparison with the XRT- and BAT-detected population. We suggest that these are mostly if not all extragalactic, though unlikely to be highly absorbed sources in the X-rays such as Compton thick AGN. A large number of these are highly variable soft X-ray (0.2–2 keV) sources and a smaller number are highly variable hard (2–12 keV) sources. A small fraction of mainly hard-band Slew Survey detections may be spurious. This follow-up programme brings us a step further to completing the identifications of a substantial sample of *XMM–Newton* Slew Survey sources, important for understanding the nature of the transient sky and allowing flux-limited samples to be constructed.

Key words: surveys – X-rays: general.

1 INTRODUCTION

The *XMM–Newton* Slew Survey (Saxton et al. 2008a) performed with the pn channel of the European Photon Imaging Camera (EPIC; Strüder et al. 2001; see also Jansen et al. 2001) is proving to be a useful resource for the discovery of bright new X-ray sources. The Slew Survey makes use of data taken while the satellite is maneuvering between pointed observations, reaching five to 10 times deeper in flux than all other all-sky spatially resolved surveys in the 2–12 keV band. It also reaches comparable sensitivity to the *ROSAT* PSPC All-Sky Survey (RASS; Voges et al. 1999, 2000) in the 0.2–2 keV band. The latest release of the clean slew catalogue (XMMSL1 – delta4) contains 11 425 sources detected over

★E-mail: rlcs1@star.le.ac.uk

28 000 deg^2 of which 72 per cent are previously known in X-rays or have plausible counterparts from other wavebands. Several interesting transients have been discovered including novae (Read et al. 2008a, 2009), tidal disruption candidates (Esquej et al. 2007) and flare stars (e.g. Read et al. 2008b; Saxton et al. 2008b). However, a quarter of the *XMM–Newton* Slew Survey sources are relatively bright yet appear to have no previous, catalogued X-ray detections. Cross-correlation with the RASS showed that of order 50 per cent of the Slew Survey point-like sources do not have RASS counterparts.

Potential explanations for the lack of previous X-ray detections of these Slew Survey sources include transient or highly variable X-ray behaviour (perhaps such sources are seen in a 'high' state during the *XMM–Newton* observations) or hard X-ray spectra (meaning that most of the counts fall outside the *ROSAT* energy range). Further possibilities include an inaccurate Slew Survey position: the 1σ position error is 8 arcsec but this has a long tail (see fig. 6 of Saxton et al. 2008a); or spurious detections: $\sim$4 per cent of the sources in the clean Slew Survey catalogue are expected to be spurious from statistical considerations (Saxton et al. 2008a). It is important to try and complete the identifications of the *XMM–Newton* Slew Survey catalogue, so as to allow flux-limited samples to be drawn from the survey and to develop a fuller picture of the X-ray transient source population.

Here we present follow-up observations of a sample of unidentified *XMM–Newton* Slew Survey X-ray sources with the *Swift* satellite (Gehrels et al. 2004). We attempt to classify the sources by obtaining more accurate localizations with the *Swift* X-Ray Telescope, measuring any X-ray variability and where possible identifying the broad-band spectral properties using all instruments on-board *Swift* and information from published optical, near-infrared (nIR) and radio catalogues. The main body of the paper details the sample, our analyses and general results. Discussion of individual sources is given in the appendix.

2 SAMPLE SELECTION

We selected our sample from the XMMSL1 catalogue (2007 August) to include sources which, in either the full (0.2–12 keV), hard (2–12 keV) or soft (0.2–2 keV) bands: (a) were detected with likelihood $\geq$10, (b) were detected with $\geq$4 counts, (c) had a low value of fitted source extent (best band extent $\leq$10 pixels) and (d) were not consistent with any known source in a multiple-catalogue search (including SIMBAD, NED and RASS to within 30 arcsec, see table 6 of Saxton et al. 2008a for the complete list). This resulted in 97 sources, of which 94 have *Swift* pointed observations and are presented here. Full-band (0.2–12 keV) X-ray fluxes for the sample, as given in the XMMSL1 catalogue, range from $\sim$(2–30) $\times$ 10^{-12} erg cm^{-2} s^{-1} and the sources are distributed apparently randomly across the sky (Fig. 1).

3 *SWIFT* OBSERVATIONS

We observed the 94 sources defined in Section 2 with all instruments on-board *Swift* simultaneously: the wide field of view Burst Alert Telescope (BAT; Barthelmy et al. 2005) operating in the energy range 15–150 keV, and the narrow-field instruments – the X-Ray Telescope (XRT; Burrows et al. 2005) and the Ultraviolet–Optical Telescope (UVOT; Roming et al. 2005). The observations with XRT (Table 1) were designed to be performed in photon counting (PC) mode and to have a minimum exposure time of 1.8 ks, to obtain an improved X-ray position and some spectral information. These
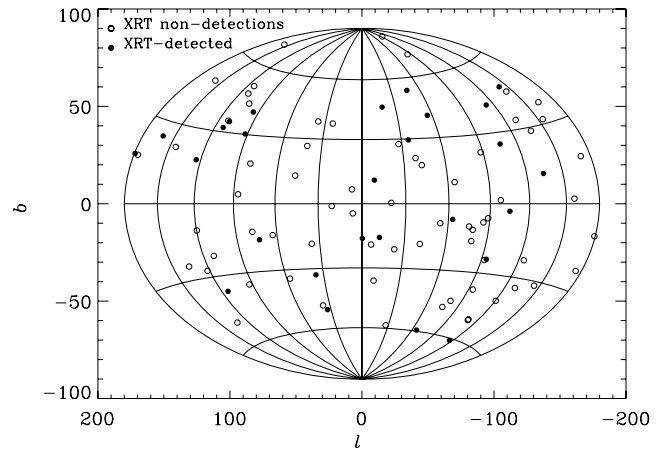

Figure 1. Aitoff projection in Galactic coordinates of the distribution of unidentified *XMM–Newton* Slew Survey sources in our sample, both *Swift* XRT detected (using the new XRT positions) and undetected (using the *XMM–Newton* Slew Survey positions).

observations were performed as 'fill-in' targets which can be over-ridden when *Swift* slews to higher priority targets such as gamma-ray bursts, resulting in exposure times varying from 240 up to 10 220 s. The total exposure time per source may have been continuously accumulated or be spread over a number of months, from 2006 August to 2009 December. Where possible, observations with the UVOT have been carried out using the *b* filter to optimize UVOT-enhanced X-ray position determination (described in Section 4.1). BAT data from the pointed observations have been combined with data from the BAT 58-month Survey (Baumgartner et al., in preparation, see also Tueller et al. 2010) to increase detection likelihood.

4 X-RAY RESULTS

We analysed the data according to the recipes given in Evans et al. (2009) and based on the publicly available *Swift* data analysis tools at http://www.swift.ac.uk/user_objects. All observations were reduced and analysed homogeneously, using the *Swift* software version 3.4 (HEASOFT 6.7) and latest calibration files as of 2009 November 1. For a detection we require a source significance above the background of 3σ. To be considered a match, the XRT-detected source position must agree with the Slew Survey position when adopting 3σ positional uncertainties. We detect 27 of the 94 observed sources with the XRT, corresponding to a detection rate of 29 per cent. The mean count rate for the detected sources is 0.038 count s^{-1}, while the mean detection limit is 0.003 count s^{-1} (Table 1), corresponding to a 0.3–10 keV flux of 10^{-13} erg cm^{-2} s^{-1} for an absorbed power law with $\Gamma = 2$ and $N_{\rm H} = 10^{21}$ cm^{-2}.

4.1 Position improvement

From the *XMM–Newton* Slew Survey, X-ray positions were measured for this sample to accuracies of $\sim$10 to $\sim$2 arcsec (radius, 1σ, including systematic error). For the detected sources the mean 90 per cent confidence X-ray positional error radius derived from the *Swift* data is 2.9 arcsec (statistical+systematic, Table 2), i.e. significantly improved compared to the 18.9 arcsec mean *XMM–Newton* Slew Survey uncertainty. Positions determined by the XRT can be improved in both accuracy and precision by using the UVOT to accurately determine the spacecraft pointing (see Goad et al. 2007; Evans et al. 2009, for full details of this procedure); this method was

Table 1. *Swift* XRT observations of unidentified *XMM–Newton* Slew Survey sources. XRT count rates are PC mode 0.3–10 keV with 1σ errors, or 3σ upper limits where no source was detected at $\geq 3\sigma$ significance (in which case no error is given). The *XMM–Newton* Slew Survey bands are described in Section 2.

Source	Slew count rate (count s⁻¹)			*Swift* obsID	Date – obs start, end	$T_{\exp}$ (ks)	XRT count rate/U. lim. (count s⁻¹)
	Full	Hard	Soft				
XMMSL1 J002202.9+254004	2.6 ± 0.7	–	2.0 ± 0.5	00037850	2008 August, 2009 June	2.38	0.138 ± 0.005
XMMSL1 J003023.0+515845	2.4 ± 0.8	2.7 ± 0.8	–	00037851	2008 May, June	3.69	$\leq 1.57 \times 10^{-3}$
XMMSL1 J004712.3+353738	0.8 ± 0.3	1.0 ± 0.4	–	00035862	2007 June	1.96	$\leq 3.30 \times 10^{-3}$
XMMSL1 J010654.8+802740	1.8 ± 0.4	–	1.6 ± 0.4	00037861	2008 September	2.72	0.016 ± 0.003
XMMSL1 J011407.7+124648	1.9 ± 0.6	–	1.7 ± 0.3	00037857	2008 August, 2009 June	2.12	$\leq 2.23 \times 10^{-3}$
XMMSL1 J012240.2−570859	1.6 ± 0.5	–	1.3 ± 0.4	00035821	2007 March, December	2.86	0.043 ± 0.004
XMMSL1 J014957.3+365200	1.7 ± 0.8	2.0 ± 1.0	–	00035810	2008 February	3.27	$\leq 2.14 \times 10^{-3}$
XMMSL1 J025808.2−651845	1.8 ± 0.6	–	1.0 ± 0.4	00035808	2006 November, 2007 December	5.33	$\leq 1.64 \times 10^{-3}$
XMMSL1 J030006.6−381617	1.4 ± 0.3	–	1.0 ± 0.3	00035842	2006 November	2.03	0.021 ± 0.003
XMMSL1 J033952.5−651256	1.3 ± 0.4	0.8 ± 0.4	–	00037873	2008 October	6.36	$\leq 1.02 \times 10^{-3}$
XMMSL1 J034923.7−433330	1.2 ± 0.3	–	1.0 ± 0.3	00037877	2008 October	2.36	$\leq 4.55 \times 10^{-3}$
XMMSL1 J035115.5−434049	1.6 ± 0.5	–	1.1 ± 0.4	00037862	2008 October, December	2.51	$\leq 2.78 \times 10^{-3}$
XMMSL1 J043707.5+112538	1.5 ± 0.7	–	–	00035828	2007 March	2.33	$\leq 2.50 \times 10^{-3}$
XMMSL1 J044357.4−364413	2.4 ± 0.6	–	1.5 ± 0.5	00035791	2006 August	2.24	$\leq 3.31 \times 10^{-3}$
XMMSL1 J045937.1−153256	1.0 ± 0.4	1.1 ± 0.5	–	00035858	2006 August, 2008 April	4.43	$\leq 1.57 \times 10^{-3}$
XMMSL1 J045949.8−573514	1.3 ± 0.5	1.4 ± 0.5	–	00035849	2006 August	2.18	$\leq 4.02 \times 10^{-3}$
XMMSL1 J050801.1−284113	1.7 ± 0.5	–	1.3 ± 0.4	00035815	2006 August, 2008 February	2.64	$\leq 2.20 \times 10^{-3}$
XMMSL1 J050824.5+220834	2.1 ± 0.6	–	–	00035795	2006 September	3.05	$\leq 2.67 \times 10^{-3}$
XMMSL1 J060339.9−294302	3.5 ± 1.0	–	1.4 ± 0.6	00035786	2006 October	2.54	$\leq 2.29 \times 10^{-3}$
XMMSL1 J060730.8+691832	1.8 ± 0.8	–	1.2 ± 0.5	00035805	2006 August	2.34	$\leq 3.16 \times 10^{-3}$
XMMSL1 J063950.7+093634	1.4 ± 0.5	–	1.2 ± 0.3	00037869	2008 August	1.86	$\leq 3.13 \times 10^{-3}$
XMMSL1 J064041.6−582308	1.2 ± 0.3	–	0.4 ± 0.2	00037878	2008 November	2.10	$\leq 2.76 \times 10^{-3}$
XMMSL1 J064109.2−565542	1.4 ± 0.4	–	1.0 ± 0.3	00037870	2008 October	5.56	0.039 ± 0.003
XMMSL1 J064849.0+394715	1.1 ± 0.3	–	1.0 ± 0.3	00035845	2008 January	5.89	$\leq 9.86 \times 10^{-4}$
XMMSL1 J065525.2+370815	2.5 ± 0.4	0.5 ± 0.2	1.8 ± 0.3	00035789	2006 October, 2008 January	3.25	0.027 ± 0.006
XMMSL1 J070846.2+554905	1.5 ± 0.6	–	–	00035787	2006 October, 2007 January	3.84	0.067 ± 0.004
	3.1 ± 0.6	0.6 ± 0.2	2.3 ± 0.4				
XMMSL1 J071111.8+280314	2.6 ± 0.8	–	1.2 ± 0.5	00037849	2009 May	1.02	$\leq 6.84 \times 10^{-3}$
XMMSL1 J075818.9−062723	–	–	2.6 ± 1.2	00035835	2007 February, April	5.35	0.020 ± 0.002
XMMSL1 J080849.0−383803	1.4 ± 0.4	–	1.0 ± 0.2	00037871	2008 June, July	1.78	0.063 ± 0.006
XMMSL1 J082730.0−672401	3.9 ± 0.6	0.6 ± 0.2	3.2 ± 0.6	00037847	2008 December, 2009 January	2.20	$\leq 3.17 \times 10^{-3}$
XMMSL1 J083704.0+193951	1.8 ± 0.8	–	1.4 ± 0.6	00035807	2007 May	5.92	$\leq 1.37 \times 10^{-3}$
XMMSL1 J084756.4−532755	1.6 ± 0.6	–	1.2 ± 0.5	00035824	2007 February	1.66	$\leq 3.90 \times 10^{-3}$
XMMSL1 J084945.3−413706	1.7 ± 0.4	–	1.1 ± 0.3	00035811	2007 April, May	4.34	$\leq 2.32 \times 10^{-3}$
XMMSL1 J085036.8+044354	1.9 ± 0.5	1.1 ± 0.4	0.7 ± 0.3	00037860	2009 January	0.24	$\leq 3.89 \times 10^{-2}$
XMMSL1 J085155.6−570352	1.5 ± 0.4	–	1.2 ± 0.3	00035838	2007 January	2.29	$\leq 3.83 \times 10^{-3}$
XMMSL1 J085216.3+283657	1.5 ± 0.5	–	1.1 ± 0.4	00037866	2009 March	2.39	$\leq 2.71 \times 10^{-3}$
XMMSL1 J090822.3−643749	9.9 ± 0.9	1.7 ± 0.4	7.0 ± 0.8	00035781	2006 December	3.05	$\leq 2.12 \times 10^{-3}$
XMMSL1 J092118.6+015302	2.3 ± 0.6	–	1.4 ± 0.5	00035793	2007 October	2.76	$\leq 2.10 \times 10^{-3}$
XMMSL1 J093738.4−654445	1.4 ± 0.6	1.6 ± 0.6	–	00035847	2007 January, April	3.26	$\leq 2.14 \times 10^{-3}$
XMMSL1 J094156.1+163246	1.7 ± 0.5	1.8 ± 0.5	–	00035813	2007 June, 2008 June	3.56	$\leq 2.08 \times 10^{-3}$
XMMSL1 J094551.3−194352	1.6 ± 0.4	–	1.0 ± 0.4	00037863	2009 February	10.22	0.049 ± 0.002
XMMSL1 J095336.4+161231	1.5 ± 0.4	–	1.3 ± 0.4	00035837	2007 June, 2008 June	2.46	0.017 ± 0.003
XMMSL1 J100011.5+553035	1.3 ± 0.4	–	0.6 ± 0.3	00037874	2009 February	2.27	$\leq 2.85 \times 10^{-3}$
XMMSL1 J101841.7−034131	1.7 ± 0.4	–	1.1 ± 0.3	00035818	2007 December	2.03	0.014 ± 0.003
XMMSL1 J103335.6−321047	1.5 ± 0.6	–	–	00035830	2006 November	2.26	$\leq 2.57 \times 10^{-3}$
XMMSL1 J114354.8−690505	1.9 ± 0.4	1.1 ± 0.4	0.8 ± 0.3	00037858	2009 February	2.34	0.076 ± 0.006
XMMSL1 J115034.4+430453	–	1.5 ± 0.5	–	00035848	2006 October	0.59	$\leq 1.26 \times 10^{-2}$
XMMSL1 J120118.8−523000	2.0 ± 0.7	–	1.5 ± 0.5	00035798	2006 September, December	2.50	$\leq 2.33 \times 10^{-3}$
XMMSL1 J121730.8+102253	2.1 ± 0.7	–	1.6 ± 0.5	00035796	2007 June	2.68	$\leq 2.17 \times 10^{-3}$
XMMSL1 J123316.9+213224	1.1 ± 0.5	1.3 ± 0.5	–	00035851	2007 March	1.62	$\leq 4.30 \times 10^{-3}$
XMMSL1 J125522.0−221035	1.7 ± 0.4	–	1.1 ± 0.3	00035841	2007 March, December	2.92	0.033 ± 0.004
	0.6 ± 0.2	–	0.5 ± 0.2				
XMMSL1 J131651.2−084915	1.5 ± 0.5	–	1.2 ± 0.4	00035827	2006 December	3.29	0.017 ± 0.002
XMMSL1 J132442.4−712852	1.3 ± 0.4	–	0.8 ± 0.3	00037875	2009 February	1.85	$\leq 5.04 \times 10^{-3}$
XMMSL1 J134637.9+650319	2.0 ± 0.6	–	1.1 ± 0.4	00037855	2008 May	2.12	$\leq 2.74 \times 10^{-3}$
XMMSL1 J140743.6−430516	4.5 ± 0.7	1.6 ± 0.4	2.7 ± 0.4	00037846	2008 August	3.31	$\leq 2.11 \times 10^{-3}$
XMMSL1 J140924.4+675831	1.9 ± 0.7	–	1.5 ± 0.5	00035803	2006 October	2.84	$\leq 2.28 \times 10^{-3}$
XMMSL1 J141843.5−293749	1.9 ± 0.6	–	1.1 ± 0.4	00035804	2006 December	5.78	0.042 ± 0.003
XMMSL1 J142022.5−384430	5.0 ± 0.7	–	4.3 ± 0.6	00037845	2009 December	2.71	$\leq 3.12 \times 10^{-3}$
XMMSL1 J143651.4−090050	1.1 ± 0.3	–	3.8 ± 1.4	00035832	2006 September	1.34	0.045 ± 0.006

Table 1 – *continued*

Source	Slew count rate (count s^{-1})			*Swift* obsID	Date – obs start, end	$T_{\exp}$ (ks)	XRT count rate/U. lim. (count s^{-1})
	Full	Hard	Soft				
XMMSL1 J145037.6−281424	2.0 ± 0.5	–	1.8 ± 0.4	00037854	2008 September	2.43	≤4.42 × 10^{-3}
XMMSL1 J152543.6+672822	1.7 ± 0.6	1.1 ± 0.6	–	00035812	2007 January	2.26	≤4.83 × 10^{-3}
XMMSL1 J160336.7+774328	1.2 ± 0.4	1.3 ± 0.4	–	00037879	2008 June	3.36	≤2.08 × 10^{-3}
XMMSL1 J161944.0+765545	2.4 ± 0.6	–	1.0 ± 0.4	00035792	2006 October	4.60	0.035 ± 0.003
XMMSL1 J162136.0+093304	2.0 ± 0.6	–	1.1 ± 0.4	00035800	2006 August, October	7.09	≤8.20 × 10^{-4}
XMMSL1 J162533.2+632411	1.4 ± 0.5	1.2 ± 0.5	–	00035854	2007 January	2.68	0.007 ± 0.002
XMMSL1 J163439.3+184545	1.5 ± 0.5	1.5 ± 0.5	–	00037865	2008 May	1.61	≤3.62 × 10^{-3}
XMMSL1 J164212.2−293051	1.1 ± 0.4	–	1.0 ± 0.3	00035843	2007 January	2.51	0.026 ± 0.004
XMMSL1 J164456.7−450015	1.3 ± 0.3	1.2 ± 0.3	–	00037876	2009 February	3.45	2.26 × 10^{-3}
XMMSL1 J164859.4+800507	1.6 ± 0.5	–	0.7 ± 0.3	00035823	2007 January	2.32	0.031 ± 0.004
XMMSL1 J170014.4−730348	1.8 ± 0.6	–	1.0 ± 0.5	00035806	2006 September, 2007 June	5.39	≤1.63 × 10^{-3}
XMMSL1 J172700.3+181422	2.2 ± 0.4	0.7 ± 0.2	1.2 ± 0.2	00037852	2008 July	2.24	≤2.59 × 10^{-3}
XMMSL1 J173637.8−193611	2.0 ± 0.3	–	1.3 ± 0.3	00035799	2007 March, 2009 February	4.98	≤1.92 × 10^{-3}
XMMSL1 J175542.2+624903	0.9 ± 0.5	–	0.7 ± 0.3	00035844	2007 February, March	2.72	0.039 ± 0.004
	1.2 ± 0.4	–	1.0 ± 0.3				
XMMSL1 J181659.8−254219	1.6 ± 0.5	1.6 ± 0.5	–	00035819	2008 February	0.67	≤8.64 × 10^{-3}
XMMSL1 J182707.5−465626	2.2 ± 0.6	–	1.2 ± 0.5	00035794	2007 June, 2008 June	3.41	0.007 ± 0.002
XMMSL1 J182933.3+175619	1.3 ± 0.4	–	0.7 ± 0.3	00037880	2008 December, 2009 May	3.53	≤2.10 × 10^{-3}
XMMSL1 J183233.0−112539	1.0 ± 0.3	1.3 ± 0.4	–	00035850	2006 October	2.26	≤5.02 × 10^{-3}
XMMSL1 J183642.8−583857	–	1.0 ± 0.4	–	00035859	2007 March	3.68	≤1.89 × 10^{-3}
XMMSL1 J185314.2−363057	2.9 ± 0.7	–	2.2 ± 0.4	00035788	2006 October	2.71	0.044 ± 0.004
XMMSL1 J185608.5−430320	1.4 ± 0.6	–	1.2 ± 0.5	00035839	2007 April, July	4.22	≤1.65 × 10^{-3}
XMMSL1 J191028.2+495606	1.6 ± 0.3	0.5 ± 0.2	1.1 ± 0.2	00035825	2006 November	2.16	≤4.06 × 10^{-3}
XMMSL1 J200203.1−055152	4.4 ± 1.3	–	2.7 ± 0.9	00035784	2006 October	2.18	≤6.23 × 10^{-3}
XMMSL1 J203044.2−484718	2.4 ± 1.1	–	–	00035790	2006 November, 2007 March	5.44	≤1.71 × 10^{-3}
XMMSL1 J204033.2+482749	1.7 ± 0.5	0.9 ± 0.4	–	00035816	2007 March	2.49	≤3.27 × 10^{-3}
XMMSL1 J204142.3+185258	2.8 ± 0.6	1.5 ± 0.5	1.1 ± 0.4	00037848	2008 June	2.05	≤2.83 × 10^{-3}
XMMSL1 J205542.2−115756	1.5 ± 0.5	–	1.2 ± 0.4	00037867	2008 June	3.60	0.020 ± 0.003
XMMSL1 J211420.7+252419	5.6 ± 0.7	0.7 ± 0.2	4.1 ± 0.5	00035783	2006 December	2.14	0.110 ± 0.008
XMMSL1 J211506.4+305811	1.7 ± 0.6	–	–	00035817	2007 March, April	3.28	≤1.77 × 10^{-3}
XMMSL1 J213537.3+024834	1.9 ± 0.5	1.6 ± 0.5	–	00037859	2009 April	2.24	≤2.60 × 10^{-3}
XMMSL1 J215303.1−173633	1.6 ± 0.6	–	–	00035822	2007 April	2.74	≤2.54 × 10^{-3}
XMMSL1 J215905.6−201604	2.1 ± 0.4	–	1.8 ± 0.3	00037853	2008 December	3.81	0.006 ± 0.001
XMMSL1 J230652.9+213159	1.6 ± 0.7	–	–	00035820	2007 May	2.90	≤2.01 × 10^{-3}
XMMSL1 J230937.0−522529	0.9 ± 0.3	1.1 ± 0.3	–	00035857	2006 December	4.13	≤1.57 × 10^{-3}
XMMSL1 J235604.5+400726	1.5 ± 0.4	–	0.9 ± 0.3	00037864	2008 July	2.31	≤2.52 × 10^{-3}

used where possible. All but four sources have UVOT-enhanced XRT positions. The XRT positions are centred between 0.8 and 34 arcsec from the *XMM–Newton* Slew Survey central positions. The detected sources are not concentrated along the Galactic plane nor at the Galactic Centre, but appear to be randomly distributed in the sky, and are not distributed differently to the undetected sources (Fig. 1).

4.2 Comparison with previous high-energy catalogues

Using the newly derived *Swift* positions for the XRT-detected sources, we searched all major high-energy catalogues, including data from *Einstein*, *Ginga*, *ROSAT*, *ASCA*, *XMM–Newton*, *Chandra*, *BATSE*, *GRANAT*, *SAS-2* and *EUVE*. This results in 10 sources with one or more possible *ROSAT* counterparts (Table 3). In addition, the revised position of one source suggests association with another *XMM–Newton* Slew Survey object (see Table 3). We have used the 3σ error radii on the X-ray positions to search for a match, which includes the 6 arcsec (1σ) systematic error in the case of RASS, while we note that the 1.4 arcsec (90 per cent) systematic error for enhanced XRT positions (3.5 arcsec where enhancement was not possible) is already included in all reported XRT positions. One of the *ROSAT* matches has been classified as a Type I active

galactic nucleus (AGN), from both X-ray and optical observations, and lies at a redshift of $z = 0.236$ (Gioia et al. 2003). Another *ROSAT* match has been classified as an F-G-type star in the Hamburg/RASS Catalogue of optical identifications V3.0 (Zickgraf et al. 2003). The XRT-detected source coincident with this RASS star is also coincident with a second Slew Survey source not included in our sample: only one X-ray source is found in the ∼17 × 17 arcmin^2 XRT field of view, hence these two Slew Survey sources and one RASS source may all be one and the same. In order to verify this, we include this XRT-detected source in all further analysis presented here. No other *ROSAT* matches have existing classifications. We note that one of our sample sources, XMMSL1 J162533.2+632411, was not detected in the soft band in the Slew Survey and is spectrally the hardest among the XRT detected sample, making the *ROSAT* association uncertain.

4.3 X-ray spectral analysis

We created one XRT spectrum per detected source, fitted using the C-statistic (Cash 1979) in xspec. The X-ray spectral model employed was an absorbed power law, where the single absorption component N_H at $z \equiv 0$ was left to vary freely rather than set to the Galactic value to allow for sources within the Galaxy as well

Table 2. Source positions and associated errors (radius, 90 per cent containment) derived from the XRT observations. All XRT positions have been UVOT enhanced, except where indicated with *.

Source XMMSL1 J	XMM position (°)	Error (arcsec)	XRT position (°)	Error (arcsec)	Position difference (arcsec)
002202.9+254004	5.51246, 25.66780	11	5.51330, 25.66779	1.5	2.7
010654.8+802740	16.72840, 80.46115	10	16.72612, 80.45951	3.9	6.1
012240.2−570859	20.66791, −57.14976	19	20.67286, −57.15126	3.6	11.1
030006.6−381617	45.02795, −38.27129	10	45.02783, −38.27109	2.1	0.8
064109.2−565542	100.28859, −56.92840	20	100.28459, −56.93256	2.3	16.9
065525.2+370815	103.85532, 37.13737	10	103.85670, 37.13786	2.9	4.3
070846.2+554905	107.19079, 55.81748	12	107.19302, 55.81767	1.6	4.6
075818.9−062723	119.57912, −6.45650	28	119.57775, −6.45644	3.5	4.9
080849.0−383803	122.20423, −38.63413	16	122.19943, −38.63185	1.7	15.8
094551.3−194352	146.46383, −19.73120	17	146.46285, −19.73380	1.5	9.9
095336.4+161231	148.40175, 16.20851	11	148.40366, 16.20801	2.6	6.8
101841.7−034131	154.67358, −3.69182	11	154.67482, −3.69063	2.7	6.2
114354.8−690505	175.97849, −69.08476	15	175.97225, −69.08709	3.9*	11.6
125522.0−221035	193.84203, −22.17633	11	193.84293, −22.17791	3.7*	6.4
131651.2−084915	199.21291, −8.82081	11	199.21360, −8.82178	2.1	4.3
141843.5−293749	214.68130, −29.63044	12	214.68451, −29.63055	1.5	10.1
143651.4−090050	219.21416, −9.01379	26	219.22130, −9.00926	3.7	30.2
161944.0+765545	244.93372, 76.92922	22	244.91138, 76.92113	1.8	34.3
162533.2+632411	246.38844, 63.40311	20	246.38694, 63.39842	4.0	17.1
164212.2−293051	250.55056, −29.51433	11	250.55137, −29.51379	2.0	3.2
164859.4+800507	252.24682, 80.08518	26	252.18727, 80.08678	9.6	37.4
175542.2+624903	268.93855, 62.82350	12	268.94182, 62.82487	1.7	7.3
182707.5−465626	276.78128, −46.94063	19	276.78290, −46.94032	4.3*	4.1
185314.2−363057	283.30962, −36.51566	12	283.30667, −36.51574	2.2	8.5
205542.2−115756	313.92622, −11.96551	11	313.92731, −11.96643	2.0	5.1
211420.7+252419	318.58667, 25.40539	118	318.58790, 25.40603	1.8	4.6
215905.6−201604	329.77282, −20.26792	11	329.77492, −20.26781	4.1*	7.1

Table 3. Possible *ROSAT* associations, displaying agreement within the 3σ positional uncertainties.

XMM Slew name XMMSL1 J	ROSAT name	ROSAT pos. err. (arcsec)	XRT pos. err. (arcsec)	Pos. diff. (arcsec)	ID (ref.)/comments
012240.2−570859	1RXS J012245.0−570901	75	6.6	28.8	
064109.2−565542	1RXS J064106.5−565610	39	4.2	19.5	
114354.8−690505	1RXH J114353.5−690513	30	7.1	1.1	
	1RXH J114353.3−690506	24		7.5	
	1RXH J114351.8−690505	18		10.8	
141843.5−293749	1RXS J141846.1−293748	33	2.7	23.8	
143651.4−090050	1RXS J143653.7−090004	111	6.7	30.1	
161944.0+765545	1RXS J161939.9+765515	24	3.3	4.0	Star F-G (Zickgraf et al. 2003) associated with XMMSL1 J161935.7+765508
162533.2+632411	1RXS J162535.1+632333	63	7.3	26.1	No soft band detection in Slew
164212.2−293051	1RXS J164216.5−293035	129	3.6	56.4	
164859.4+800507	1RXS J164843.5+800506	27	17.5	7.4	
175542.2+624903	1RXS J175546.2+624927	21	3.1	2.8	AGN Type I, $z = 0.236$ (Gioia et al. 2003)
XMM Slew name XMMSL1 J (this sample)	XMM Slew name (possible counterpart)	XMM pos. err. (counterpart, arcsec)	XRT pos. err. (arcsec)	pos. diff. (arcsec)	ID (ref.)/comments
161944.0+765545	XMMSL1 J161935.7+765508	32	3.3	13	Star F-G (Zickgraf et al. 2003) associated with 1RXS J161939.9+765515

as extragalactic objects. Results of the spectral fits are given in Table 4, where we also list the expected Galactic extinction from the Leiden/Argentine/Bonn (LAB) H ɪ maps (Kalberla et al. 2005). In one case there was no acceptable fit.

The power-law photon indices cluster around $\Gamma = 1.5$–2.0 (Fig. 2), typical of AGN (Mateos et al. 2005, 2010; Mainieri et al. 2007). The measured equivalent hydrogen column densities with this model are consistent with or in excess of the Galactic value for

Table 4. Results of absorbed power-law fits to the X-ray spectra of XRT detected sources. $N_{H,Gal}$ is a weighted average at the XRT position (Kalberla et al. 2005). Fluxes are given for the interval 0.3–10 keV. We also list the total number of source counts in the final column.

Source XMMSL1 J	Γ	N_H $\times 10^{20}$ (cm^{-2})	$N_{H,Gal}$ $\times 10^{20}$ (cm^{-2})	Observed flux $\times 10^{-12}$ $(erg\ cm^{-2}\ s^{-1})$	Unabsorbed flux $\times 10^{-12}$ $(erg\ cm^{-2}\ s^{-1})$	C-stat (dof)	N_{counts}
002202.9+254004	$1.69^{+0.14}_{-0.19}$	$1.6^{+4.3}_{-1.6}$	3.03	$5.9^{+1.1}_{-1.5}$	6.1	209.24 (191)	328
010654.8+802740	No acceptable fit		16.0	0.34^a	–	–	43
012240.2−570859	$3.74^{+0.83}_{-0.74}$	$10.0^{+10.6}_{-8.1}$	2.96	$1.21^{+0.38}_{-0.71}$	3.1	55.26 (70)	123
030006.6−381617	$1.91^{+0.61}_{-0.33}$	Unconstrained	1.85	$0.83^{+0.34}_{-0.83}$	0.83	25.76 (33)	42
064109.2−565542	$1.73^{+0.27}_{-0.35}$	$8.2^{+5.8}_{-7.8}$	5.81	$1.62^{+0.45}_{-0.84}$	1.9	104.27 (122)	216
065525.2+370815	$2.5^{+2.4}_{-1.3}$	22^{+51}_{-22}	11.3	$0.24^{+0.15}_{-0.24}$	0.48	19.95 (18)	87
070846.2+554905	$1.80^{+0.25}_{-0.26}$	$8.2^{+3.3}_{-6.0}$	5.06	$2.97^{+0.59}_{-1.22}$	3.5	147.11 (165)	257
075818.9−062723	$1.63^{+0.45}_{-0.42}$	$9.4^{+11.7}_{-9.4}$	8.21	$0.97^{+0.33}_{-0.87}$	1.1	73.13 (81)	107
080849.0−383803	$3.24^{+0.74}_{-0.59}$	14^{+11}_{-8}	75.8	$1.76^{+0.54}_{-1.25}$	4.4	69.22 (75)	112
094551.3−194352	$1.66^{+0.19}_{-0.21}$	24^{+3}_{-7}	3.83	$2.64^{+0.45}_{-0.70}$	3.4	266.09 (273)	500
095336.4+161231	$2.31^{+1.04}_{-0.72}$	$8.7^{+21.0}_{-8.7}$	3.34	$0.61^{+0.32}_{-0.61}$	0.84	31.26 (32)	41
101841.7−034131	$2.8^{+2.5}_{-1.5}$	35^{+56}_{-33}	3.81	$0.49^{+0.31}_{-0.49}$	1.6	22.33 (22)	28
114354.8−690505	$1.66^{+0.30}_{-0.30}$	29^{+12}_{-11}	18.0	$5.8^{+1.3}_{-2.2}$	7.8	144.64 (180)	177
125522.0−221035	$1.44^{+0.41}_{-0.39}$	$5.2^{+12.7}_{-5.2}$	6.47	$1.80^{+0.70}_{-1.45}$	1.9	84.69 (57)	96
131651.2−084915	$2.89^{+1.25}_{-0.64}$	$3.5^{+15.3}_{-3.2}$	2.37	$0.48^{+0.24}_{-0.48}$	0.62	46.40 (39)	56
141843.5−293749	$1.86^{+0.27}_{-0.28}$	$8.4^{+5.8}_{-6.3}$	4.95	$1.76^{+0.42}_{-0.67}$	2.1	100.84 (154)	242
143651.4−090050	$3.1^{+1.6}_{-1.4}$	31^{+32}_{-16}	5.80	$1.37^{+0.54}_{-1.37}$	5.1	59.09 (48)	60
161944.0+765545	$4.58^{+0.86}_{-0.62}$	41^{+14}_{-16}	4.10	$0.83^{+0.24}_{-0.78}$	14.0	80.23 (90)	161
162533.2+632411	$1.05^{+0.82}_{-0.63}$	Unconstrained	1.86	$0.54^{+0.47}_{-0.54}$	0.54	14.89 (13)	18
164212.2−293051	$4.2^{+1.3}_{-1.1}$	29^{+20}_{-19}	13.5	$0.65^{+0.28}_{-0.65}$	4.9	45.85 (49)	65
164859.4+800507	$2.47^{+0.69}_{-0.60}$	17^{+17}_{-13}	4.52	$1.07^{+0.41}_{-1.07}$	1.9	52.10 (56)	72
175542.2+624903	$2.10^{+0.39}_{-0.23}$	Unconstrained	3.25	$1.42^{+0.38}_{-0.81}$	1.4	64.36 (72)	106
182707.5−465626	$1.83^{+0.92}_{-0.48}$	Unconstrained	5.99	$0.29^{+0.16}_{-0.29}$	0.29	16.56 (21)	23
185314.2−363057	$2.78^{+0.76}_{-0.68}$	16^{+15}_{-6}	6.65	$1.28^{+0.42}_{-1.13}$	2.7	75.60 (80)	119
205542.2−115756	$3.09^{+1.21}_{-0.69}$	19^{+18}_{-13}	4.49	$0.57^{+0.23}_{-0.57}$	1.6	37.15 (52)	72
211420.7+252419	$2.60^{+0.25}_{-0.33}$	11^{+7}_{-6}	7.53	$3.39^{+0.70}_{-0.95}$	5.7	83.51 (146)	235
215905.6−201604	$3.2^{+3.2}_{-1.4}$	17^{+47}_{-17}	2.47	$0.17^{+0.12}_{-0.17}$	0.49	13.57 (18)	22

^{a} Flux is taken from an unconstrained absorbed power-law fit and so is approximate. This fit had a power-law photon index of $\Gamma \sim 9.3$ and absorption $N_H \sim 10^{22}\ cm^{-2}$; blackbody and MEKAL fits also resulted in no acceptable solutions.

all sources except XMMSL1 J080849.0−383803: this source has a column far lower than the expected Galactic value and therefore probably lies close-by, within our Galaxy. We discuss the accuracy of the Galactic column in this direction in Appendix A9, where we conclude that the source is Galactic.

A power-law fit to one of the sample sources, XMMSL1 J161944.0+765545, results in a very soft photon index, $\Gamma = 4.58^{+0.86}_{-0.62}$, and no counts are detected at >5 keV. In Table 3 we have shown that XMMSL1 J161944.0+765545 is associated with the *ROSAT*-discovered source 1RXS J161939.9+765515, classed as an F-G star. An absorbed MEKAL model fit to the XRT spectrum results in a plasma temperature of $kT = 1.2^{+0.1}_{-0.2}$ keV and a total absorbing column of $\leq 2 \times 10^{20}\ cm^{-2}$ with C-statistic (dof) = 93 (90). The measured upper limit on the total column density is lower than the mean Galactic column of $4.1 \times 10^{20}\ cm^{-2}$ in that direction, consistent with its classification.

4.4 X-ray variability

The *Swift* 0.3–10 keV XRT count rates and upper limits all lie below those expected, given the catalogued full-band count rates in the

XMM–Newton Slew Survey performed 1.6–5.4 yr earlier (Fig. 3a). Many of the *Swift* XRT observations to date provide a null detection suggesting that the source has dropped in X-ray flux by a factor of 10 to 100 or more.

In order to compare the *Swift* XRT and *XMM–Newton* observations, we need to understand the relationship between the Slew Survey count rates and XRT count rates. XSPEC simulations show that the relative count rate ratio expected between *XMM–Newton* EPIC pn and XRT PC mode is 15.5:1 for a typical AGN spectrum with an X-ray absorbing column of $N_H = 3 \times 10^{20}\ cm^{-2}$ and a power-law photon index of $\Gamma = 1.7$. This may be uncertain by ± 10 per cent considering instrument cross-calibration. After accounting for this factor we still find that all sources but one have lower than expected XRT count rates at least at the 1σ level and assuming constant source flux.

In addition, the Eddington bias (Eddington 1913) should be taken into account. This can boost the true count rates of sources at or near the detection limit. Simulations performed in order to understand the *XMM–Newton* hard band survey show that those count rates can be overestimated by a factor of 2 or more in flux-limited surveys such as this. Warwick et al. (in preparation) have quantified this
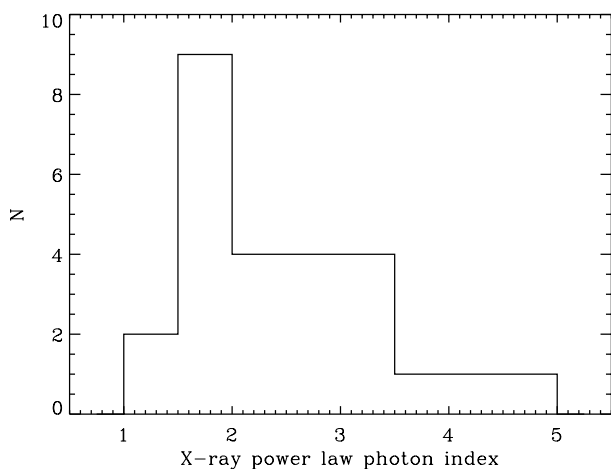
Figure 2. Distribution of XRT best-fitting power-law photon indices for the detected sources, excepting XMMSL1 J010654.8+802740.

effect for the *XMM–Newton* hard band slew survey (2–12 keV), by using the hard band $\log N - \log S$ to create source distributions, simulating Slew Survey observations of these and measuring the resultant observed count rates. For a given observed count rate they derive the true count rate distribution, which peaks a factor of 2 below the observed count rate for detections with a low number of counts (<8). Using these distributions we find an average conversion from observed to true count rates which could be applied to the Slew Survey count rates (Fig. 3b). We stress that this is at best a first-order approximation when applied to the full-band count rates.

When we compare the observed count rates of the sample in the *XMM–Newton* Slew Survey and in the *Swift* XRT follow-up, our sample appears to split into two groups (Fig. 3a). One group shows a similar count rate to that expected from the Slew Survey if count rate conversion and biases are taken into account, while the other group is composed largely of the non-detections: this latter group of sources must, if real, be significantly variable to have been seen

in the Slew Survey but not in the *Swift* XRT observations. According to the Kolmogorov–Smirnov (K–S) test, the XRT count rates for the detected sources and the upper limits on the XRT count rates for the non-detected sources are significantly different and likely not drawn from the same distribution. We discuss the XRT non-detected population further in Section 6.

Four of the XRT-detected sources show significant X-ray variability on the basis of multiple XRT observations, on time scales of days to months and by factors of 1.4–2. These are XMMSL1 J002202.9+254004, XMMSL1 J094551.3−194352, XMMSL1 J095336.4+161231 and XMMSL1 J175542.2+624903. A comparison of the average XRT soft band (0.3–2 keV) observed fluxes for XRT-detected sources with the RASS fluxes or upper limits identifies three sources which have varied by a factor of 3 or more on 15–19 yr time scales: XMMSL1 J002202.9+254004, XMMSL1 J030006.6−381617 and XMMSL1 J094551.3−194352. The population as a whole includes both increases and decreases in flux since the RASS observations.

5 BROAD-BAND CHARACTERIZATION OF X-RAY DETECTED SOURCES

5.1 Hard X-ray detections with *Swift* BAT

The wide field of the BAT hard X-ray detector on-board *Swift* means that our sample sources were in the BAT field of view on more occasions than the XRT observations listed in Table 1; these data have been compiled in the BAT 58-month Survey (Baumgartner et al., in preparation). Although none of the sources was detected above the 4.8σ survey threshold, five sources were detected at $>3.0\sigma$ significance. These sources and their 15–150 keV BAT count rates are listed in Table 5. Two of the five sources, XMMSL1 J002202.9+254004 and XMMSL1 J185608.5−430320, were also detected by the XRT. The limiting BAT count rate on the non-detected sources is typically $2.4 \times 10^{/5}$ count cm^{-2} s^{-1} (1σ, $\sim$0.1 mCrab). All but one (XMMSL1 J093738.4−654445) of the
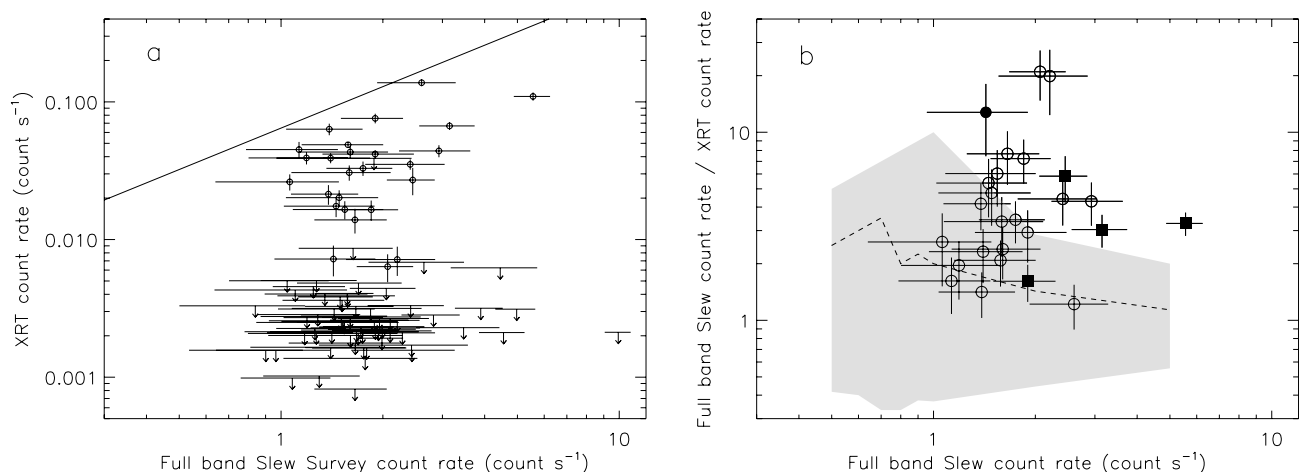

Figure 3. (a) Observed *XMM–Newton* pn count rate versus observed *Swift* XRT count rate (open circles and 1σ error bars for XRT detections, upper limits for XRT non-detections). The solid line shows a 15.5:1 ratio which is expected for the transformation between count rate for the two instruments (Section 4.4). (b) The ratio between the *XMM–Newton* Slew Survey and XRT full band count rates after correcting for the expected 15.5:1 count rate ratio factor. Open circles denote soft band Slew Survey detections, filled circles denote hard band Slew Survey detections and filled squares denote hard+soft band Slew Survey detections. The shaded area and dashed line indicate the values expected (full range and at peak, respectively, see Section 4.4 for details) for non-variable sources from Eddington bias simulations performed for the *XMM–Newton* Slew hard band survey. The location of points both within and outside of the shaded area shows that the XRT-detected population likely comprises both steady and substantially variable sources.

Table 5. BAT detections in the 58-month hard X-ray survey. The significance of the detection is given by σ.

Source XMMSL1 J	σ	Count rate ×10⁻⁵ (count cm⁻² s⁻¹)	Flux ×10⁻⁵ (mCrab)	XRT detected?
002202.9+254004	3.3	7.8 ± 2.2	0.31	Y
044357.4−364413	3.1	4.6 ± 1.9	0.21	N
093738.4−654445	3.0	7.0 ± 2.1	0.27	N
125522.0−221035	3.2	8.1 ± 2.7	0.36	Y
185608.5−430320	4.0	10.0 ± 2.7	0.44	N

five sources is at high Galactic latitude ($|b| > 20°$). While X-ray binaries, pulsars, magnetic cataclysmic variables (CVs) and Be/symbiotic stars can show very high energy X-ray and γ-ray emission, extragalactic sources are likely to be more numerous among the BAT detections. For example, Landi et al. (2010) carried out *Swift* follow-up observations of 20 unidentified *INTEGRAL*/IBIS sources and found that 11 of these could be classified as extragalactic – AGN, quasi-stellar objects (QSOs) and a low-ionization nuclear emission-line region (LINER). Only one of their sample was confirmed to be a Galactic object.

The two BAT-detected sources that are also seen in the X-ray band with XRT have coincident optical sources which lie at the faint end of the sample range and have no measured proper motion (Sections 5.2 and 5.3). We suggest these are likely extragalactic jet-dominated sources such as blazars. The low BAT detection rate we find here is inconsistent with these sources being heavily obscured (Compton thick) AGN. Winter et al. (2009) show that the BAT 9-month AGN Survey is complete down to a 2–10 keV flux of 1.0×10^{-11} erg cm⁻² s⁻¹ with a 4.8σ threshold (fig. 15 of Winter et al. 2009). Since the BAT Survey sensitivity is dominated by statistics, the 58-month survey will go deeper by a factor of 2.5, and if we accept sources down to 3.0σ, BAT should detect all AGN down to 2.4×10^{-12} erg cm⁻² s⁻¹, which is below the $\sim 4 \times 10^{-12}$ 2–12 keV sensitivity of the *XMM–Newton* Slew Survey. Furthermore, it is unlikely that more than a small fraction of the AGN would be so variable as to be bright at the time of the *XMM–Newton* Slew Survey detection and undetectable by either XRT or BAT a few years later. Blazars, however, are known to have bright X-ray flares and tend to have a soft spectrum in the BAT energy range, making them relatively difficult to detect.

Four of the five BAT-detected sources were detected only in the soft and full bands in the Slew Survey. One source, XMMSL1 J093738.4−654445, was not detected in the soft band but only in the hard and full bands in the Slew Survey. Hard band only (2–12 keV) Slew Survey detections amount to ∼20 per cent of the full sample, most of which are not detected with *Swift* XRT rendering the nature of this population rather difficult to determine (but see Section 6). We note that a hard-only Slew Survey source not a member of our sample, XMMSL1 J171900.4−353217 which has been designated as a hard X-ray flash, was observed and detected with *Swift* XRT (Armas Padilla et al. 2010; Read et al. 2010). It is located in the Galactic ridge and has been shown to be transient in nature through multiple X-ray observations. The hard BAT-detected Slew Survey source in this sample, XMMSL1 J093738.4−654445, lies at low Galactic latitude, $b = -10$, and could be a Galactic hard X-ray transient candidate, while the remaining members could be blazars or other AGN types.

5.2 Optical and UV detections with *Swift* UVOT

A single UVOT source lies within the revised XRT error circle for the majority of the XRT-detected Slew Survey sources. We derived positions for and performed photometry on these sources using the *Swift* tool UVOTDETECT. The results are presented in Table 6, where magnitudes are uncorrected for extinction and do not include any systematic uncertainties associated with the zero-points (Poole et al. 2008) but positional errors include a systematic uncertainty of 0.42 arcsec (Breeveld et al. 2010). 24 of the XRT-detected sources are observed in the *b* filter, and 16 sources have UV observations. There are a handful of very bright sources with $b < 14$, while the mean *b* magnitude is 16.4. Approximate limiting magnitudes for the UVOT for these sources are $20 < b < 11$, consistent with the upper and lower bounds of the reported magnitudes. For completeness we include in Table 6 sources that we classified in Section 4.2.

5.3 Matches with catalogued optical and nIR sources

The UVOT spatial resolution is based on a point spread function full width at half-maximum (FWHM) of ∼2.2–3.0 arcsec, which might result in blends of two or more optical sources appearing as one object. To further pinpoint and characterize the optical sources found with UVOT we searched the Two Micron All Sky Survey (2MASS; Cutri et al. 2003), USNO-B1.0 (Monet et al. 2003), USNO-A2.0 (Monet 1998) and Naval Observatory Merged Astrometric Dataset (NOMAD; Zacharias et al. 2005, including information from the unpublished USNO YB6 Catalog) catalogues, via the VizieR search engine, to look for objects within the XRT error circles. This resulted in either single matches for which we report the *BVRIJHK* magnitudes and any measured proper motions in Table 7, or in three cases no single match was found. We compared the UVOT *b* magnitude with the USNO.B1 *B* magnitude for those sources for which both measurements are available. This comparison suggests that in the majority of cases the UVOT source and the catalogued source are likely to be the same object. The sources may be optically variable (quite likely given that many are X-ray variable) so this is only an indication of correspondence, but all sources with catalogued magnitudes of $B \sim 19$ or brighter are of similar magnitude to the UVOT detected source. At the faint end of the catalogued magnitude distribution we find two sources with UVOT counterparts two magnitudes or more brighter than the corresponding catalogued source. In these cases, either UVOT measures a different source, cannot resolve a blend of multiple sources, is detecting variability or one or both of the measured magnitudes are incorrect.

Where there is a match with a single catalogued and identified source, we can further refine our sample. Four sources can be classified through this method, assuming that the catalogued match is the optical counterpart of the X-ray detected source. These are indicated in Table 7 and comprise one QSO at redshift $z = 0.87$, two high proper-motion stars one of which likely lies at $d < 33$ pc and one variable star with a period of 0.7 d. We expect a number of flare stars to be included in this sample, given that they are both populous and highly variable.

The X-ray to optical flux ratio is often used as a method of classification of galaxies (e.g. Hornschemeier et al. 2001; Laird et al. 2009, and references therein). Here we calculated

$$\log(F_X/F_R) = \log F_X + 5.5 + R/2.5, \tag{1}$$

where F_X is the 0.3–10 keV observed X-ray flux with XRT and *R* is taken from the observed magnitudes in the USNO-B1.0 catalogue. The ratios we derive are listed in Table 7 and plotted in Fig. 4:

Table 6. UVOT photometry (observed magnitudes from a sum of all images), where a single source lies inside XRT error circle of XRT-detected objects, and best source position in degrees as measured from all of the UVOT filters. Positional errors are at the 90 per cent confidence level. For comparison, we list the Galactic extinction expected in the *B* band, A_B at λ 4400 Å, for each source (Schlegel, Finkbeiner & Davis 1998).

Source XMMSL1 J	T_{exp} (ks)	A_B (mag)	b (λ4392 Å)	uvw1 (λ2600 Å)	uvm2 (λ2246 Å)	uvw2 (λ1928 Å)	Position (°)	Error (arcsec)	Dist. from XRT (arcsec)
002202.9+254004	0.40	0.12	18.29 ± 0.06	–	–	–	5.51283, 25.66771	0.43	1.5
	1.95		17.56 ± 0.02	–	–	–	5.51281, 25.66764	0.42	1.7
010654.8+802740	2.68	1.09	15.531 ± 0.005	–	–	–	16.73078, 80.45952	0.42	2.8
012240.2−570859	0.36	0.09	–	18.81 ± 0.07	–	–	20.67407, −57.15148	0.43	2.5
030006.6−381617	0.96	0.08	18.98 ± 0.05	–	–	17.38 ± 0.03	45.02705, −38.27077	0.42	2.5
064109.2−565542	5.46	0.28	19.03 ± 0.02	–	–	–	100.28361, −56.93271	0.42	2.0
065525.2+370815	0.41	0.39	17.34 ± 0.03	–	–	15.28 ± 0.02	103.85636, 37.13712	0.42	2.9
	1.30		–	–	–	19.58 ± 0.09	103.85645, 37.13704	0.42	3.0
070846.2+554905	0.55	0.22	14.525 ± 0.007	–	–	–	107.19354, 55.81770	0.42	1.1
	1.28		14.463 ± 0.004	–	–	15.59 ± 0.01	107.19360, 55.81768	0.42	1.2
080849.0−383803	2.00	8.28	12.692 ± 0.003	–	–	–	122.19961, −38.63166	0.42	0.9
	0.08		12.70 ± 0.01	–	–	–	122.19957, −38.63173	0.42	0.6
094551.3−194352	4.47	0.22	17.204 ± 0.008	–	–	–	146.46257, −19.73377	0.42	1.0
	5.61		17.167 ± 0.007	–	–	–	146.46251, −19.73378	0.42	1.2
095336.4+161231	1.10	0.15	–	15.76 ± 0.02	-	–	148.40346, 16.20807	0.42	0.7
	1.58		–	–	15.80 ± 0.02	–	148.40345, 16.20807	0.42	0.8
101841.7−034131	2.01	0.17	–	–	–	18.75 ± 0.06	154.67424, −3.69100	0.44	2.5
125522.0−221035	0.49	0.44	18.59 ± 0.04	–	–	17.00 ± 0.03	193.84352, −22.17781	0.43	2.0
131651.2−084915	1.56	0.15	18.97 ± 0.05	–	–	18.93 ± 0.08	199.21316, −8.82206	0.42	1.9
141843.5−293749	2.86	0.32	18.52 ± 0.03	–	–	17.47 ± 0.02	214.68418, −29.63034	0.42	1.3
161944.0+765545	2.22	0.17	13.814 ± 0.003	–	–	17.31 ± 0.03	244.91057, 76.92112	0.42	0.7
162533.2+632411	1.29	0.11	19.64 ± 0.07	–	–	19.05 ± 0.07	246.38582, 63.39865	0.43	2.0
164212.2−293051	1.20	1.35	14.930 ± 0.006	–	–	–	250.55113, −29.51355	0.42	1.2
175542.2+624903	0.42	0.15	17.20 ± 0.03	–	–	16.06 ± 0.02	268.94131, 62.82506	0.42	1.1
	0.69		17.14 ± 0.02	–	–	15.87 ± 0.02	268.94127, 62.82493	0.42	0.9
182707.5−465626	3.3	0.28	–	–	18.58 ± 0.06	–	276.78193, −46.93987	0.44	2.9
185314.2−363057	1.31	0.47	16.29 ± 0.01	–	–	–	283.30690, −36.51562	0.42	0.8
205542.2−115756	3.55	0.24	13.584 ± 0.002	–	–	–	313.92706, −11.96664	0.42	1.2
211420.7+252419	1.02	0.44	16.47 ± 0.01	–	–	15.43 ± 0.01	318.58768, 25.40623	0.42	1.0
215905.6−201604	3.76	0.12	15.868 ± 0.005	–	–	–	329.77498, −20.26761	0.42	0.8

five sources cannot be evaluated this way because four sources do not have *R*-band observations and one source has no acceptable X-ray model fit. The log of the ratio of X-ray to optical fluxes results in values ranging from −2.05 to 1.30. AGN (both broad and narrow line) typically show $-1 < \log(F_X/F_R) < 1$ (Hornschemeier et al. 2001; Laird et al. 2009), while lower values are obtained for low-luminosity AGN, starbursts and normal galaxies (e.g. Barger et al. 2002) and stars where an M star is expected to have $\log(F_X/F_R) = -2$ (Hornschemeier et al. 2001). Of the 22 sources we tested in this sample, 15 have classic AGN-like ratios. Five sources have $\log(F_X/F_R) < -1$, XMMSL1 J080849.0−383803, XMMSL1 J161944.0+765545, XMMSL1 J101841.7−034131, XMMSL1 J164212.2−293051 and XMMSL1 J205542.2−115756. The first two of these we have classified as stars, while the remaining three have optical magnitudes among the brightest in the sample suggesting these may also be stellar in nature. Two sources have $\log(F_X/F_R) > 1$, XMMSL1 J002202.9+254004 and XMMSL1 J030006.6−381617, and both of these have BAT detections possibly consistent with a contribution to the high energy emission from a jet (e.g. a blazar) though we note that magnetic CVs can also have large X-ray to optical flux ratios.

We caution first that the X-ray fluxes we use are often based on low signal-to-noise ratio spectra and a power law is not the only model that may provide a good fit to the data. Second, we have not corrected for the unknown amount of extinction and absorption along the line of sight to the sources so we are not calculating the intrinsic flux ratios. Third, we have to make the assumption that the catalogued *R*-band sources are indeed the optical counterparts to our X-ray detected sources and that no variability has occurred between the ground-based and *Swift* XRT observations.

Seven of the sources have substantial measured proper motions (>20 or <-20 mas yr^{-1}), indicating that these must be relatively nearby stars. In Fig. 5 we plot a colour–colour diagram using the 2MASS magnitudes and their errors for the catalogued sources, and compare these to the main sequence to see if any sources may be identified as stellar. We find that nine sources lie along the main sequence for A- through M-type stars. None of the sources could be of earlier stellar type according to their nIR colours. Six of these nine sources have significant proper motions and five have X-ray to optical flux ratios lower than expected for AGN, supporting the classification of these as main-sequence stars. In fact, we find that two sources are associated with known stars from the coincidence of the UVOT and catalogued source positions (Table 7).

5.3.1 Optical spectroscopy

An optical spectrum for XMMSL1 J064109.2−565542 was obtained at the 3.6-m New Technology Telescope (NTT) at La Silla, Chile on 2010 March 8. Two exposures of 600 s each were made with the ESO Faint Object Spectrograph and Camera (EFOSC2) in good weather conditions, covering the wavelength range from ~4500 to 7500 Å at 12 Å resolution. Details of the observational set-up and

Table 7. Optical/nIR photometry of catalogue matches with USNO-B1.0 (*BRI*, if not available then we use USNO-A2.0), YB6 USNO unpublished catalogue reported in NOMAD (*V*) and 2MASS (*JHK*), where a single source lies within the XRT error circle. Distances from the XRT error circle. Distances from the XRT position are taken from the 2MASS source if available, otherwise from USNO-B1.0. Proper motions (PM) are quoted from the NOMAD data base.

Source XMMSL1J	Dist. (arcsec)	B	V	R	I	J	H	K	PM? (mas yr⁻¹)	log $\frac{F_X}{F_R}$	Catalogued name (VizieR) and ID
002202.9+254004	1.3	18.02	17.96	17.46	17.26	16.43 ± 0.12	15.89 ± 0.16	14.69 ± 0.11	N	1.25	
010654.8+802740	1.2	15.17	14.28^a	13.16	10.63	9.35 ± 0.02	8.77 ± 0.03	8.52 ± 0.02	202 ± 0, −30 ± 2	−1.70	NLTT 3583 high proper motion M star at $d < 33$ pc
012240.2−570859	2.5	18.88	–	18.56	18.71	–	–	–	N	1.01	
030006.6−381617	2.3	19.40	17.590	19.71	18.44	–	–	–	N	1.30	
064109.2−565542	1.8	21.08	–	17.96	18.11	17.02 ± 0.22	16.28 ± 0.24	15.05 ± 0.14	N	0.89	
065525.2+370815	2.7	20.70	–	–	–	–	–	–	N	–	
070846.2+554905	1.3	14.73	13.49	13.76	13.19	11.84 ± 0.02	11.33 ± 0.03	11.20 ± 0.02	2 ± 3, 4 ± 1	−0.52	
075818.9−062723	2.9	20.60	–	17.76	17.38	–	–	–	N	0.59	
080849.0−383803	0.7	11.75	11.19	10.53	10.03	8.75 ± 0.02	8.12 ± 0.04	7.94 ± 0.03	−40 ± 2, 93 ± 2	−2.04	ASAS J080848−3837.9 variable star with $P = 0.7$ d
094551.3−194352	1.5	17.38	16.57	16.51	16.08	15.64 ± 0.08	15.34 ± 0.12	15.20 ± 0.17	−14 ± 4, −48 ± 2	0.53	
095336.4+161231	0.3	17.28	15.79	16.65	16.52	15.64 ± 0.06	15.32 ± 0.10	14.60 ± 0.08	N	−0.05	SDSS J095336.86+161228.8 quasar at $z = 0.87$
101841.7−034131	2.5	15.08	–	13.91	12.62	11.64 ± 0.02	11.05 ± 0.02	10.86 ± 0.02	−15 ± 9, −6 ± 9	−1.24	
114354.8−690505	–	–	–	–	–	–	–	–	–	–	
125522.0−221035	1.8	19.93	–	17.30	17.96	16.29 ± 0.10	15.40 ± 0.09	14.53 ± 0.09	N	0.68	
131651.2−084915	2.2	18.16	17.25	17.70	17.13	17.06 ± 0.26	15.61 ± 0.15	14.55 ± 0.11	N	0.26	
141843.5−293749	1.5	17.07	17.64	17.27	16.63	16.02 ± 0.08	15.10 ± 0.07	14.24 ± 0.07	N	0.65	
143651.4−090050	3.9	20.55	18.00	18.00	17.47	–	–	–	222 ± 49, −218 ± 70	0.84	USNO-B1.0 0809−0268143 high proper motion star
161944.0+765545	0.5	13.67	12.38	11.33	10.35	9.36 ± 0.02	8.72 ± 0.02	8.51 ± 0.02	−62 ± 3, −110 ± 2	−2.05	
162533.2+632411	2.3	18.76	17.97	18.66	18.03	16.86 ± 0.18	16.26 ± 0.22	15.64 ± 0.24	N	0.69	
164212.2−293051	1.2	14.26	13.06	12.33	11.00	10.26 ± 0.03	9.64 ± 0.04	9.37 ± 0.03	0 ± 7, −40 ± 7	−1.76	
164859.4+800507	–	–	–	–	–	–	–	–	–	–	
175542.2+624903	0.6	16.76	–	16.28	15.64	15.56 ± 0.06	14.60 ± 0.06	13.61 ± 0.05	N	0.16	
182707.5−465626	1.8	16.96	16.61	16.36	15.71	16.04 ± 0.12	15.38 ± 0.14	14.56 ± 0.12	−8 ± 2, −4 ± 23	−0.49	
185314.2−363057	1.0	15.45	–	13.72	12.14	11.12 ± 0.02	10.45 ± 0.02	10.24 ± 0.02	4 ± 5, −32 ± 5	−0.90	
205542.2−115756	1.2	13.19	12.51	11.98	11.20	10.41 ± 0.02	9.77 ± 0.02	9.61 ± 0.02	7 ± 5, −13 ± 5	−1.95	
211420.7+252419	1.0	16.23	15.50	15.43	15.21	14.81 ± 0.05	14.01 ± 0.06	13.01 ± 0.04	−1 ± 5, 4 ± 6	0.20	
215905.6−201604	–	–	–	–	–	–	–	–	–	–	

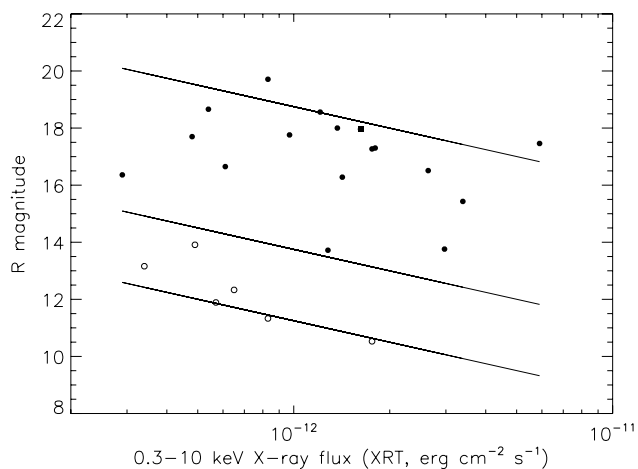^{a}From LSPM catalogue, see Appendix A2.

Figure 4. X-ray to optical flux ratios for XRT-detected sources with potential catalogued *R*-band counterparts. The solid lines indicate $\log(F_X/F_R)$ of 1 (upper line) and -1 (middle line), between which AGN are typically found (filled circles), and -2 (lower line) which extends this diagnostic to low-luminosity AGN, starbursts and normal galaxies (open circles). The square symbol indicates a source with a $b \rightarrow B$ mismatch.
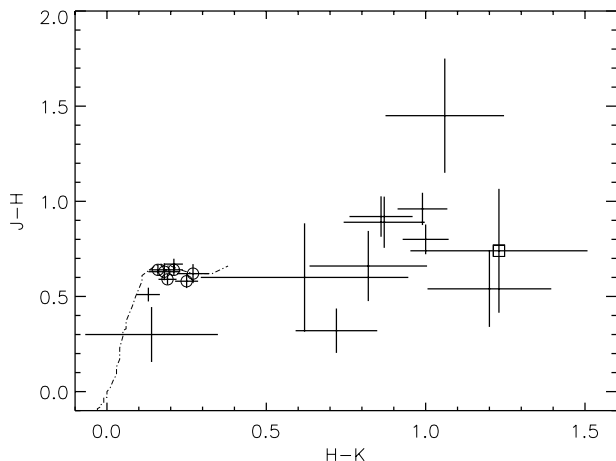

Figure 5. 2MASS colours for the objects which lie within XRT error circles, where only one unclassified source is listed. Magnitudes do not include any correction for extinction. The dot–dashed line indicates the expectation for A- through M-type main-sequence stars (Bessell & Brett 1998; Allen 2000). Open circles are overlaid on sources with $\log(F_X/F_R) < -1$ as depicted in Fig. 4. The square symbol indicates a source with a $b \rightarrow B$ mismatch.

data reduction are given in Appendix A5. The object is classified as a broad-line AGN, based on the detection of a broad (FWHM > 1000 km s^{-1}) Hβ 4861 Å line, at a redshift of $z = 0.368 \pm 0.001$ (from the detection of the [O II] λ3727, [O III] λ 4959 and [O III] λ5007 emission lines) as shown in Fig. 6. We plan to establish or confirm the classifications presented in this work with optical spectroscopy of all previously unclassified optical counterparts to the XRT-detected sources.

5.4 Matches with catalogued radio sources

We searched the radio catalogues available via VizieR on all the XRT- and BAT-detected sources to look for radio associations within 30 arcsec of the XRT- and BAT-detected sources. Only one object, XMMSL1 J164859.4+800507, has an associated radio source listed in the Atlas of Radio/X-ray Associations (ARXA; Flesch 2010), the
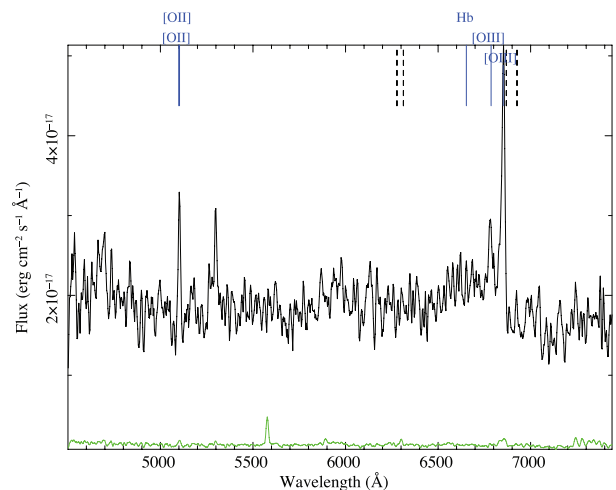
Figure 6. NTT-EFOSC2 optical spectrum for XMMSL1 J064109.2−56554 (black) and sky background spectrum underneath (grey), corrected for Galactic reddening, showing the optical emission lines used for the identification of the source. Atmospheric absorption lines are indicated with dashed lines.

Westerbork Northern Sky Survey (WENSS; Rengelink et al. 1997) and the 1.4 GHz NRAO VLA Sky Survey (NVSS; Condon et al. 1998). The lack of an optical detection for this source with *Swift* UVOT is consistent with the approximate reported *B* magnitude in the ARXA of 19.9. The ARXA also reports an *R* magnitude of 16.2, implying that the source is extremely red perhaps due to dust extinction or high redshift, or it is highly variable since the *R* and *B* magnitudes were not necessarily obtained at the same epoch.

We then searched the VLA Faint Images of the Radio Sky at Twenty-cm catalogue (FIRST; White et al. 1997), MIT-Green Bank 5-GHz Survey Catalog (Griffith et al. 1991, and references therein), Sydney University Molonglo Sky Survey (SUMSS; Mauch et al. 2003), WENSS (Leiden 1998) and NVSS (Condon et al. 1998) catalogues for radio emission within a few arcseconds of any of the *Swift*-detected sources. Again, only XMMSL1 J164859.4+800507 has associated radio emission: NVSS 164843+800516 lies 5.8 arcsec away, within the XRT error circle, and has an integrated 20 cm (1.4 GHz) flux density of 3.8 ± 0.5 mJy. Three further radio sources are located in this region, between 8 arcsec and 1.5 arcmin distant: WN 1652.5+8009, WN 1652.5+8009A and WN 1652.5+8009B with 92 cm (325 MHz) flux densities spanning 30–80 (±2) mJy.

XMMSL1 J164859.4+800507 has proven difficult to classify given its relatively poor positional uncertainty and lack of any clear optical counterpart, so the association with a radio source at 20 cm will play a major role determining the nature of this object. Interestingly, the candidate blazars XMMSL1 J002202.9+254004 and XMMSL1 J125522.0−221035, highly X-ray variable sources with large X-ray to optical flux ratios (the latter also detected with *Swift* BAT), are not associated with any known radio sources, within the scope of our search.

6 XRT-UNDETECTED SOURCES

The majority of our sample of unidentified X-ray sources from the *XMM–Newton* Slew Survey are not detected with *Swift*. While the nature of these sources is difficult to determine, it is very important to attempt to do so in order to understand the complete population identified by the Slew Survey. We expect to pick up large

numbers of transients due to the requirement that sample sources were not already identified from a variety of multiwavelength catalogue searches (Section 2). We only required a detection in one of the three Slew Survey energy bands, with a minimum of four source counts, so we also expect that some fraction of these identifications will be spurious.

First, we address the issue of spurious detections. Statistical considerations leads to an estimate of 4 per cent that are expected to be spurious sources in the *XMM–Newton* Slew Survey clean catalogue (Saxton et al. 2008a). This figure does not apply directly to our sample, as it was calculated on full-band detections and for the entire catalogue (i.e. without applying the source selection criteria used here), but can be used as a guide. The *XMM–Newton* full-band detection likelihoods of our sample range from 10 to 556 (for details see Saxton et al. 2008a). The mean detection likelihoods for the XRT-detected and XRT non-detected sources are 37 and 32, respectively, i.e. the confidence in these detections is approximately equal for an average source from each population, using this measure alone.

We searched the 2MASS catalogue for bright nIR sources coincident with the *XMM–Newton* Slew Survey positions (the nIR being less susceptible to extinction than optical bands). We found that 27 per cent of the XRT non-detected Slew Survey sources have one or more catalogued nIR sources brighter than $J = 14$ mag within 15 arcsec. To estimate the fraction for which this will be true simply by chance, we generated 10000 random sky positions and cross-correlated these with the 2MASS catalogue. This leads to the expectation that a 2MASS source brighter than $J = 14$ mag will appear within 15 arcsec of a random sky position around 7.9 per cent of the time. The fraction expected by chance is therefore much lower than obtained for our sample of XRT non-detected sources. We can conclude from this that some fraction of our non-detected subset must be real. For our XRT-detected subset, only 30 per cent of the sources would have been recovered when performing the same $J < 14$ mag cut; for example in the case of flare stars we expect only the closest sources to be found this way. So finding a bright nIR counterpart strongly suggests the X-ray source is real, while the lack of a counterpart is not constraining.

We then investigated the distribution of our detected and non-detected subsets over the Slew Survey energy bands. Sources can appear in any one of the hard (2–12 keV), soft (0.2–2 keV) and full (0.2–12 keV) bands, or could appear in multiple bands. Sources that appear in all three bands we term hard+soft. Fig. 7 shows the numbers of detected (shaded areas) and non-detected sample sources that are hard (only), soft (only), full (only) or hard+soft band detections in the Slew Survey against the number of measured counts per source. We see that most of the samples were soft only (soft or soft+full band) Slew Survey detections, reflecting the observed X-ray source population in general. We also expect a greater number of objects with low numbers of counts in the Slew Survey soft band than in the hard band because, (a) many of these sources are expected to be unabsorbed AGN: their emission is greater in the soft band and follows a power law such that sources close to the detection limit may appear soft-only, and (b) the background is higher in the hard band making source detection more difficult. The bright nIR counterpart search described above returned a match for XRT non-detected sources from the hard, soft and hard+soft categories, in the ratios 1.0:2.5:0.2 (for comparison, all XRT non-detected sources follow the ratios 1.0:1.65:0.2 for the same bands).

There are 11 sources detected in all three Slew Survey bands, and we can be confident that these sources are all astrophysical yet only 36 per cent are *Swift* detected. This suggests that a significant
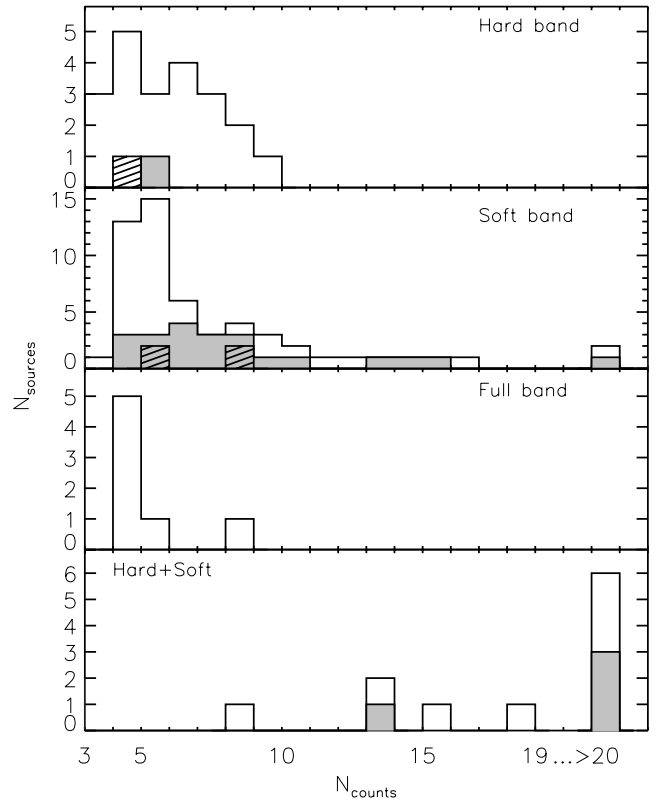

Figure 7. The numbers of BAT/XRT-detected (grey shading for XRT detections, hatching for BAT detections) and non-detected sample sources against the number of measured counts reported in the *XMM–Newton* Slew Survey observation. The four panels show the distribution over the Slew Survey energy bands: hard or hard+full band (2–12 keV, top), soft or soft+full band (0.2–2 keV, upper middle), full band only (0.2–12 keV, lower middle) and hard+soft+full bands (lower panel).

fraction of the XRT non-detected sample is highly variable sources. Of the 55 soft-only sources, 22 are XRT detected, a further two are BAT detected and a further 12 have $J < 14$ mag nIR sources within 15 arcsec. From our estimates, described earlier, $\sim$ two of the soft-only sources may be coincident with a $J < 14$ mag nIR source by chance. We can therefore say that at least 34 out of 55 (62 per cent) are likely to be real astrophysical sources. The remaining 38 per cent may comprise 30 per cent with J-band counterparts below the brightness cut we imposed, following the proportion seen in the XRT-detected source population; just 8 per cent or approximately four sources are then left unaccounted for and could potentially be spurious. Of the 21 hard-only sources, just one is detected with XRT and one is detected with BAT. A further five have bright nIR sources in the vicinity of which one–two may be chance coincidences. If we again adopt the fraction 30 per cent for real sources likely to have nIR counterparts fainter than $J = 14$, we find 38 per cent of all the XRT/BAT-non-detected hard-only sources would be considered real. This provides an upper bound on the fraction of hard-only sample sources that are potentially spurious. Full band only Slew Survey sources comprise 10 per cent of the XRT non-detected sources. We have found no catalogued bright, nearby J-band sources for this subsample. In summary, there are likely to be some spurious sources included in the full-only and hard-only subsamples, while the vast majority if not all the soft-only sources as well as all the hard+soft sources are probably astrophysical.

We now focus on the nature of the XRT non-detected sources. The distribution on the sky of XRT non-detected sources appears very similar to that of the detected sources (Fig. 1). The median of the Galactic column densities, $N_{H,Gal}$, in those directions is not significantly different for the detected and non-detected samples, but we note that this could have hampered the detection of XMMSL1 J164456.7−450015 and XMMSL1 J183233.0−112539 which may lie behind particularly large Galactic columns of 1.65×10^{22} and 1.13×10^{22} cm^{-2}, respectively. The lack of detections with *Swift* BAT argues against a population of heavily obscured AGN (Section 5.1). To support this we compared expected XRT count rates for typical AGN at $z = 0.1$ with observed 0.3–10 keV flux 10^{-12} erg cm^{-2} s^{-1}, power-law photon index $\Gamma = 1.7$, Galactic column density $N_H = 10^{20}$ cm^{-2} and intrinsic X-ray absorbing columns of $N_H = 10^{21}$, 10^{22} and 10^{23} cm^{-2}, and find the count rate is reduced by 64 per cent at most, which is not enough to push these sources into our XRT non-detected category. An intrinsic column density of $N_H = 10^{24}$ cm^{-2} is required to bring the 0.3–10 keV XRT count rate for this spectral shape down to the mean detection limit for this sample.

We require greater variability among the non-detected sources, shown in Fig. 3(a), with variability corresponding to flux changes of up to a factor of ∼300. These highly variable sources remain an enigma and are likely to do so until they are seen again, perhaps as they undergo an X-ray outburst or otherwise enter a high flux state.

7 DISCUSSION AND CONCLUSIONS

Swift observations of a sample of 94 unidentified X-ray sources from the *XMM–Newton* Slew Survey have been carried out, with 29 per cent of the sample sources detected with XRT. This low detection rate supports the hypothesis that many of these sources are highly variable or X-ray transient objects. The X-ray emission or upper limit to the emission for all the sources, taking into account count rate conversion between instruments and Eddington bias, lies at or below that seen in the Slew Survey. Up to two-thirds of the XRT detected sources could have remained constant in flux between the Slew Survey and *Swift* observations. Approximately one-third of the XRT detected sources and also the majority of the XRT non-detected sources are likely to be variable.

The X-ray positions we derived from the *Swift* data for the XRT-detected sources improved the mean 90 per cent confidence error radius from 18.9 to 2.9 arcsec. This reduced the number of UVOT and catalogued optical matches to just a single source in most cases. Performing a new cross-correlation of the 3σ error radii with multiwavelength catalogues revealed that six sources can be associated with known objects and eight sources may be associated with unidentified *ROSAT* sources. The X-ray spectrum of most of the sources can be fit with an absorbed power law with photon indices clustering around $\Gamma = 1.5$–2.0, typical of AGN. The random distribution across the sky of this and the non-detected population is also consistent with an AGN classification. To identify the types of objects included in the XRT detected sample we used a number of further indicators: the X-ray to optical flux ratio, proper motion, nIR colours, radio associations and detection in γ-rays with BAT. We summarize the proposed source classifications in Table 8. We find 10 of the 30 XRT- and/or BAT-detected sources are clearly stellar in nature, including one periodic variable star and two high proper motion stars. 11 sources are classified as AGN, four of which are detected in hard X-rays with BAT and three of which have redshifts spanning $z = 0.2$–0.9 obtained from the literature or from optical spectroscopy. A further three sources are suspected

Table 8. Summary of proposed classifications for individual sources, and/or any associated catalogued sources.

Source	Proposed identification	Associated catalogued sources
XMMSL1 J002202.9+254004	AGN, possible blazar	
XMMSL1 J010654.8+802740	M-type star	NLTT 3583
XMMSL1 J012240.2−570859	AGN, possible NLS1	1RXS J012245.0−570901
XMMSL1 J030006.6−381617	Possible AGN	
XMMSL1 J044357.4−364413	Possible AGN	
XMMSL1 J063950.7+093634	Possible periodic M star, $P = 1.36$ d	See Appendix A4
XMMSL1 J064109.2−565542	Type I AGN, $z = 0.368$	1RXS J064106.5−565610
XMMSL1 J065525.2+370815	Possible QSO	
XMMSL1 J080849.0−383803	Periodic variable star, $P = 0.72$ d	ASAS J080848−3837.9
XMMSL1 J093738.4−654445	Candidate Galactic hard X-ray flash	
XMMSL1 J094551.3−194352	Flare star	
XMMSL1 J095336.4+161231	QSO, $z = 0.87$	SDSS J095336.86+161228.8
XMMSL1 J101841.7−034131	M star	
XMMSL1 J114354.8−690505	–	Multiple *ROSAT* matches
XMMSL1 J125522.0−221035	AGN, possible blazar	
XMMSL1 J131651.2−084915	AGN	
XMMSL1 J141843.5−293749	AGN	1RXS J141846.1−293748
XMMSL1 J143651.4−090050	High proper motion star	USNO-B1.0 0809−0268143/1RXS J143653.7−090004
XMMSL1 J161944.0+765545	Late-type m-s star	XMMSL1 J161935.7+765508/1RXS J161939.9+765515
XMMSL1 J162533.2+632411	AGN, possible Type II	
XMMSL1 J164212.2−293051	M star	1RXS J164216.5−293035
XMMSL1 J164859.4+800507	Possible AGN	1RXS J164843.5+800506/NVSS 164843+800516
XMMSL1 J175542.2+624903	Type I AGN, $z = 0.236$	1RXS J175546.2+624927
XMMSL1 J182707.5−465626	Possible AGN	
XMMSL1 J185314.2−363057	Possible M star	
XMMSL1 J185608.5−430320	Possible AGN	
XMMSL1 J205542.2−115756	K-M type star	
XMMSL1 J211420.7+252419	Possible AGN	

AGN and one is a candidate Galactic hard X-ray flash, while five sources remain unclassified. Interestingly, the two most variable sources on time scales of a few years (between the *XMM–Newton* and *Swift* observations) are among those which we cannot classify here. We plan to obtain optical spectroscopy where possible for all these sources, which will confirm or determine their identifications, as demonstrated in Section 5.3.1 for XMMSL1 J064109.2−565542.

The XRT/BAT non-detected population are equally important to classify, but the lack of information makes this task far more difficult. The majority of these are likely highly variable sources, and from the lack of BAT detections we can to a large extent rule out a population of heavily obscured AGN. We also expect some fraction of these sources may be spurious detections. We compared the non-detected population with the detected population in terms of the distribution of *XMM–Newton* Slew Survey counts in each of the hard, soft and full bands. The X-ray error circles from the Slew Survey are somewhat large for a full optical/nIR counterpart search, so instead we looked for bright nIR sources within 15 arcsec of the Slew Survey position, and compared this to the number expected in a chance coincidence. Combining these two sets of information, we estimate the fraction of astrophysical sources as opposed to spurious detections among the XRT non-detected population for each Slew Survey band. All the hard+soft band detections are extremely likely to be real, and we find that most if not all the soft sources are also likely to be real; 73 per cent of all sample sources fall into these two categories. Perhaps 60 per cent of the 21 hard-only sources could be spurious. We stress, however, that these figures are only estimates and there is potential for as yet unknown source types within these populations. It is likely that the nature of each *Swift* non-detected source will remain elusive until they are once again detected, permitting further study.

In summary, the XRT-detected population seems to consist of approximately equal numbers of X-ray active stars and background AGN, while the undetected population may contain more extragalactic objects such as AGN. Type II AGN were perhaps expected to be the dominant population due to their lack of soft X-ray emission, given that this sample was selected based on *ROSAT* soft X-ray non-detections, but we identify only one possible Type II candidate among the XRT-detected population. Neither are they numerous among the XRT non-detected sources as implied by the lack of BAT detections. A knowledge of the source types detected in surveys such as the *XMM–Newton* Slew Survey is important for investigation of the $\log N - \log S$ and completing studies of the X-ray background that cannot be done with pointed observations alone. Follow-up of the Slew Survey sources with *Swift* has also enabled the identification of a highly variable population, largely of unknown nature.

ACKNOWLEDGMENTS

REFERENCES

Adelman-McCarthy J. K. et al., 2009, The SDSS Photometric Catalog, Release 7. VizieR On-line Data Catalog

Allen C. W., 2000, in Cox A. N., ed., Allen's Astrophysical Quantities, 4th edn. AIP Press, New York

Armas Padilla M., Degenaar N., Yang Y., Patruno A., Wijnands R., 2010, Astron. Telegram, 2656

Barthelmy S. et al., 2005, Space Sci. Rev., 120, 143

Berger A. J., Cowie L. L., Brandt W. N., Capak P., Garmire G. P., Hornschemeier A. E., Steffen A. T., Wehner E. H., 2002, AJ, 124, 1839

Bessell M. S., Brett J. M., 1988, PASP, 100, 1134

Böhringer H. et al., 2004, REFLEX Galaxy Cluster Survey Catalogue. VizieR On-line Data Catalog

Breeveld A. A. et al., 2010, MNRAS, 406, 1687

Burrows D. N. et al., 2005, Space Sci. Rev., 120, 165

Cash W., 1979, ApJ, 228, 939

Condon J. J., Cotton W. D., Greisen E. W., Yin Q. F., Perley R. A., Taylor G. B., Broderick J. J., 1998, AJ, 115, 1693

Cutri R. M. et al., 2003, The IRSA 2MASS All-Sky Point Source Catalog. NASA/IPAC Infrared Science Archive

Eddington A. S., 1913, MNRAS, 73, 359

Esquej P., Saxton R. D., Freyberg M. J., Read A. M., Altieri B., Sanchez-Portal M., Hasinger G., 2007, A&A, 462, L49

Evans P. A. et al., 2009, MNRAS, 397, 1177

Flesch E., 2010, Publ. Astron. Soc. Australia, 27, 283

Gehrels N. et al., 2004, ApJ, 611, 1005

Gioia I. M., Henry J. P., Mullis C. R., Böhringer H., Briel U. G., Voges W., Huchra J. P., 2003, ROSAT North Ecliptic Pole Survey. VizieR On-line Data Catalog

Goad M. R. et al., 2007, A&A, 476, 1401

Griffith M., Heflin M., Conner S., Burke B., Langston G., 1991, ApJS, 75, 801

Hamuy M., Suntzeff N. B., Heathcote S. R., Walker A. R., Gigoux P., Phillips M. M., 1994, PASP, 106, 566

Henry J. P., Mullis C. R., Voges W., Böhringer H., Briel U. G., Gioia I. M., Huchra J. P., 2006, ApJS, 162, 304

Hornschemeier A. E. et al., 2001, ApJ, 554, 742

Jansen F. et al., 2001, A&A, 365, L1

Jones D. et al., 2009, MNRAS, 399, 683

Kalberla P. M. W., Burton W. B., Hartmann D., Arnal E. M., Bajaja E., Morras R., Pöppel W. G. L., 2005, A&A, 440, 775

Laird E. S. et al., 2009, ApJS, 180, 102

Lamm M. H., Mundt R., Bailer-Jones C. A. L., Herbst W., 2005, A&A, 430, 1005

Landi R., Bassani L., Malizia A., Stephen J. B., Bazzano A., Fiocchi M., Bird A. J., 2010, MNRAS, 403, 945

Lepine S., Shara M. M., 2005, LSPM-North Catalog. VizieR On-line Data Catalog

Mainieri V. et al., 2007, ApJS, 172, 368

Mateos S. et al., 2005, A&A, 433, 855

Mateos S. et al., 2010, A&A, 510, 35

Mauch T., Murphy T., Buttery H. J., Curran J., Hunstead R. W., Piestrzynski B., Robertson J. G., Sadler E. M., 2003, MNRAS, 342, 1117

Mickaelian A. M., Hovhannisyan L. R., Engels D., Hagen H.-J., Voges W., 2006, Optical Identification of ROSAT-FSC Sources. VizieR On-line Data Catalog

Monet D. G., 1998, USNO-A2.0. United States Naval Observatory

Monet D. G. et al., 2003, AJ, 125, 984

Poole T. S. et al., 2008, MNRAS, 383, 627

Read A. M. et al., 2008a, A&A, 482, L1

Read A. M., Saxton R. D., Osborne J. P., Pye J., Evans P. A., 2008b, Astron. Telegram, 1718

Read A. M. et al., 2009, A&A, 506, 1309

Read A. M., Saxton R. D., Esquej P., Evans P. A., 2010, Astron. Telegram, 2627

Rebull L. M. et al., 2002, AJ, 123, 1528

Rengelink R. B., Tang Y., de Bruyn A. G., Miley G. K., Bremer M. N., Roettgering H. J. A., Bremer M. A. R., 1997, A&AS, 124, 259

Roming P. W. A. et al., 2005, Space Sci. Rev., 120, 95

Saxton R., Read A. M., Esquej P., Freyberg M. J., Altieri B., Bermejo D., 2008a, A&A, 480, 611

Saxton R., Read A. M., Esquej P., Freyberg M., 2008b, Astron. Telegram, 1361

Schlegel D. J., Finkbeiner D. P., Davis M., 1998, ApJ, 500, 525

Souchay J. et al., 2009, A&A, 494, 799

Strüder L. et al., 2001, A&A, 365, L18

Tueller J. et al., 2010, ApJS, 186, 378

Voges W. et al., 1999, A&A, 349, 389

Voges W. et al., 2000, ROSAT All-Sky Survey Faint Source Catalog. VizieR On-line Data Catalog

Watson C., Henden A. A., Price A., 2009, AAVSO International Variable Star Index VSX. VizieR On-line Data Catalog

White R. L., Becker R. H., Helfand D. J., Gregg M. D., 1997, AJ, 475, 479

Winter L. M., Mushotzky R. F., Reynolds C. S., Tueller J., 2009, ApJ, 690, 1322

Zacharias N., Monet D. G., Levine S. E., Urban S. E., Gaume R., Wycoff G. L., 2005, NOMAD Catalog. VizieR On-line Data Catalog

Zickgraf F.-J., Engels D., Hagen H.-J., Reimers D., Voges W., 2003, Hamburg/RASS Catalogue of Optical Identification, V3.0. VizieR On-line Data Catalog

APPENDIX A: NOTES ON INDIVIDUAL SOURCES

A1 XMMSL1 J002202.9+254004

Two *Swift* pointed observations were taken 10 months apart, during which we see significant variability in both the X-ray (count rate increasing by a factor of ~5) and optical (an increase of 1 mag) bands. This, together with a high X-ray to optical flux ratio, suggests this is a blazar whose X-ray emission is boosted by contributions from a jet, while the lack of a radio association casts doubt on this classification.

A2 XMMSL1 J010654.8+802740

This source is detected with the XRT with one of the lowest count rates of the sample though Galactic absorption in this direction is very high. The signal-to-noise ratio in the X-ray spectrum is very low and we cannot model the spectral shape but we find that this source is X-ray variable on time scales of a few years. A bright UVOT counterpart is present despite having the second highest reddening among the detected sources equating to 1.09 mag in *B* band. We note that the *V* magnitude listed in NOMAD for this source, $V = 17.8$, is inconsistent with the LSPM-North proper-motion catalogue of nearby stars (Lepine & Shara 2005), listing of $V = 14.28$ and the latter is a more reasonable extrapolation of catalogued magnitudes in other wavebands.

A3 XMMSL1 J012240.2−570859

If this source is an AGN, the blue colour and soft X-ray spectrum may indicate a large soft X-ray excess and a strong big blue bump suggestive of a narrow-line Seyfert 1 galaxy.

A4 XMMSL1 J063950.7+093634

This source is not detected with *Swift*. We note the presence of a $J \sim 14$ M-type variable star in the galaxy NGC 2264 with period 1.36 d

at 5 arcsec distance from the *XMM–Newton* Slew Survey position, within the error circle (Rebull et al. 2002; Lamm et al. 2005).

A5 XMMSL1 J064109.2−565542

An optical spectrum for this source was obtained at the NTT, La Silla (Chile) on 2010 March 8. Observing conditions were good with sky transparency clear to photometric and a seeing of ~1 arcsec. Two exposures of 600 s each at an airmass of 1.1 were made with the EFOSC2 with a 1 arcsec slit width oriented at the parallactic angle and grating 4, covering the wavelength range from ~4500 to 7500 Å at 12 Å resolution (from unblended arc lines taken through the slit at ~6000 Å). A standard reduction process was applied using IRAF routines. Wavelength calibration was carried out by comparison with exposures of a helium–argon arc lamp, with an accuracy <1 Å. Relative flux calibration was carried out by observations of the spectrophotometric standard star LTT 3218 (Hamuy et al. 1994). We estimate an error on the flux calibration <10 per cent from the standard adjustment during the calibration procedure. The spectrum has been corrected for Galactic reddening. The object is classified as a broad-line AGN, based on the detection of a broad (FWHM >1000 km s^{-1}) Hβ 4861 Å line, at a redshift of 0.368 ± 0.001 (from the detection of the [O II] $\lambda3727$, [O III] $\lambda4959$ and [O III] $\lambda5007$ emission lines) as shown in Fig. 6.

A6 XMMSL1 J065525.2+370815

Using the approximate X-ray flux from the power-law spectral fit, we compared this to the flux during the *XMM–Newton* Slew Survey observation and find significant variability of a factor of at least 20. Consistent with the position of the UVOT counterpart we find an optical counterpart listed in USNO-B1.0 of order 3 mag fainter in *B* than the UVOT source. This source is also listed in Sloan Digital Sky Survey (SDSS) Data Release 7 (DR7), where its magnitude is approximately the same as derived from the UVOT observations. This source is therefore variable in both X-ray and optical wavebands.

A7 XMMSL1 J070846.2+554905

The XRT flux is among the highest in the sample, and the spectrum is well fitted with a power law of photon index 1.8, typical of AGN, while the absorption is non-zero and consistent with the Galactic absorption in that direction. A very small proper motion is reported in the catalogues searched, and the nIR colours are consistent with a K-type main-sequence star. However, the X-ray to optical flux ratio is consistent with an AGN. This source will remain unclassified until optical spectroscopy can be obtained.

A8 XMMSL1 J075818.9−062723

The UVOT *b* and USNO *B* magnitudes for this source differ by 2.5 mag, indicating either large variability or inaccurate photometry. The X-ray spectrum is seen to harden between the *XMM–Newton* and *Swift* observations, being formally detected only in the soft band with *XMM–Newton* but seen in the full *Swift* energy band. The X-ray to optical flux ratio lies right in the middle of the expected range for AGN while the absence of any nIR emission which is uncommon for an AGN. This source requires further observations in order to determine its nature.

A9 XMMSL1 J080849.0−383803

This source is very likely Galactic because the X-ray column density measured in a spectral fit ($0.15 \pm 0.10 \times 10^{22}$ cm^{-2}) is lower than the Galactic column in that direction of 0.78×10^{22} cm^{-2} (Kalberla et al. 2005). The LAB H I maps show that this high Galactic column exists both at the nearest measured position to the XRT position, 0°.06 away and is the result with weighted interpolation over all the nearest measured values within a $1°$ radius. The LAB Survey is the most sensitive Milky Way H I survey to date, with the most extensive coverage both spatially and kinematically. We extracted the X-ray flux seen by RASS at the new XRT enhanced X-ray position (Table 2) and using the spectral shape measured by XRT (Table 4) and recover a detection. The X-ray flux appears to have decreased by 60 per cent over 17.7 yr. The UVOT-enhanced X-ray position we derive, with error radius 1.7 arcsec (90 per cent containment) corresponds to a bright UVOT source of *b* magnitude 12.69. Its catalogued optical and nIR colours match those of a late K star, and this source has a proper motion typical of a thin disc star. The X-ray to optical flux ratio also suggests a stellar nature for this source. The position coincides with that of ASAS J080848−3837.9, a variable star listed in the AAVSO International Variable Star Index VSX (Watson, Henden & Price 2009) of unknown type but with a period of 0.72 d.

A10 XMMSL1 J090822.3−643749

This source is not detected with *Swift* despite showing the highest full-band *XMM–Newton* pn count rate of the entire sample of 9.9 ± 0.9 count s^{-1} (most of the counts fell in the soft band). The XRT detection limit was 0.002 count s^{-1}, indicating a factor of at least 100 decrease in X-ray flux between the *XMM–Newton* observations in 2004 and the *Swift* observations in 2006 at flux levels of $\sim 3 \times 10^{-11}$ to $< 1 \times 10^{-13}$ erg cm^{-2} s^{-1}, respectively (assuming a typical AGN spectrum). *XMM–Newton* slewed over this position on two further occasions, in 2002 and 2008, during which the source was not detected to full-band limits of ≤ 0.4 and ≤ 0.3 count s^{-1}, respectively.

A11 XMMSL1 J094156.1+163246

This source is not detected with *Swift*. We note, however, that a SDSS galaxy with measured redshift of $z = 0.17$ lies within the 3σ error circle at 40-arcsec radius.

A12 XMMSL1 J094551.3−194352

This source is detected with XRT and UVOT. The X-ray position has been determined at the most accurate level achieved for this sample, with a 90 per cent error radius of 1.5 arcsec. Multiple *Swift* observations show variability, decreasing by a factor of 1.4 in soft X-ray flux on time scales of days, and the spectrum has hardened in the 2.2 yr between the *XMM–Newton* and XRT observations. We extracted the X-ray flux seen by RASS at the new XRT enhanced X-ray position (Table 2) and using the spectral shape measured by XRT (Table 4) and recover a detection. A comparison of the 0.3–2 keV XRT flux with the RASS flux at the XRT position shows significant variability: a factor of $4.2^{+0.6}_{-0.8}$ (1σ error) increase over 18 yr.

A13 XMMSL1 J095336.4+161231

This source is detected with XRT and UVOT. The X-ray spectral shape is poorly constrained, but the X-ray and optical fluxes are of the same order suggesting this is an AGN. At the XRT position there is a known quasar: SDSS J095336.86+161228.8 which lies at a redshift of $z = 0.87$ (Adelman-McCarthy et al. 2009). The XRT observations span 1 yr, during which time the source halved in X-ray flux.

A14 XMMSL1 J114354.8−690505

The X-ray flux at the time of the XRT observation of this source is approximately the same as measured with *XMM–Newton* and twice that measured at the XRT position with *ROSAT*, 5 and 18.6 yr previously, respectively. Three *ROSAT* HRI sources lie within the 3σ XRT error circle, listed in Table 3. The *ROSAT* reported count rates for all of these sources are almost identical: 0.029 ± 0.005, 0.028 ± 0.005 and 0.027 ± 0.005 count s^{-1}, respectively, and it is not clear which object, if indeed these are distinct objects, corresponds to the XRT- and *XMM–Newton*-detected X-ray source. Given the lack of optical and radio information it is difficult to classify this source.

A15 XMMSL1 J125522.0−221035

The X-ray source was observed twice with *XMM–Newton*, both times only formally detected in the soft band. Comparison of the X-ray flux as observed with XRT, *XMM–Newton* and *ROSAT* reveals variability: the source is at least three times brighter in XRT than in *ROSAT* observations 17 yr earlier (in the *ROSAT* pass band) and doubled in flux in the 2.4 yr between the two *XMM–Newton* observations. The *b*-band magnitude measured with UVOT is 1.5 mag brighter than the catalogued *B* value, again indicating variability. All indicators used in this study point to an extragalactic source.

A16 XMMSL1 J131651.2−084915

The UVOT magnitudes lie at the faint end of the UVOT detectability range, while the longer wavelength catalogued magnitudes at the same position are somewhat higher and show that this is a red object. The XRT X-ray flux has decreased to a tenth of the *XMM–Newton*-observed value. We extracted the X-ray flux seen by RASS at the new XRT enhanced X-ray position (Table 2) using the spectral shape measured by XRT (Table 4) and recover a detection. No variability is detected between the XRT and RASS observations 16.4 yr apart. We note the optical flux and spectral shape are very similar to that of XMMSL1 J141843.5−293749, which we suggest is an AGN, while the X-ray flux is three times lower.

A17 XMMSL1 J141843.5−293749

The XRT position for this source has the best accuracy achieved in this sample, with an error radius of 1.5 arcsec (90 per cent containment). The X-ray flux during the XRT observation was at least two times lower than observed with *XMM–Newton* but approximately the same as that of the associated *ROSAT* source.

A18 XMMSL1 J143651.4−090050

This source, classified here as a high proper motion star, is ~ 12 arcsec from a galaxy cluster at $z = 0.08$ (Böhringer et al. 2004; Jones et al. 2009).

A19 XMMSL1 J161944.0+765545

This source is detected with XRT and UVOT. The XRT refined position is coincident both with the *ROSAT* source 1RXS J161939.9+765515 and with the *XMM–Newton* Slew Survey source XMMSL1 J161935.7+765508. The Slew Survey source 161935.7+765508 is not part of our sample due to its association with 1RXS J161939.9+765515. In the $\sim 17 \times 17$ arcmin^2 field of view of XRT only one X-ray source is detected, and its UVOT-enhanced X-ray position (with a 90 per cent error radius of 1.8 arcsec), lies 13 arcsec from the *XMM–Newton* position of 161939.9+765515 (90 per cent error radius of 18 arcsec) and 34 arcsec from that of 161944.0+765545 (90 per cent error radius of 22 arcsec). Within their 3σ error circles these three positions are all consistent, and are most probably one and the same source. The Hamburg/RASS Catalog of optical identifications V3.0 (Zickgraf et al. 2003) provides an F-G star classification for the bright optical counterpart to the RASS source, 2MASS J16193872+7655165, which lies within the XRT error circle. The *Swift* XRT X-ray spectrum is not well fitted with an absorbed power law, requiring a very soft photon index of $\Gamma \sim 4.6$ and a high absorbing column of order 4×10^{22} cm^{-2} (10 times higher than the Galactic column). We performed, instead, an absorbed MEKAL fit to these data, giving a plasma temperature of $kT = 1.2^{+0.1}_{-0.2}$ keV and an upper limit on the total column density lower than the mean Galactic column, suggesting this source is located between us and the far side of our Galaxy. The X-ray to optical flux ratio we measure places this source outside the region of typical AGN, and the nIR colours show that it is consistent with being a late-type main-sequence star as reported by Zickgraf et al. (2003).

A20 XMMSL1 J162136.0+093304

This source is not detected with *Swift*. We note that this field has been observed with *Swift* for 7.09 ks, with no detection to a deep 3σ upper limit of 8.2×10^{-4} count s^{-1}.

A21 XMMSL1 J162533.2+632411

This source is detected with XRT and has a faint UVOT counterpart. The X-ray spectral parameters are difficult to constrain, however, this is spectrally the hardest detected XRT and was detected only in the full band and hard bands in the *XMM–Newton* Slew Survey. We see variability in the X-ray flux of at least a factor of 3 on a time-scale of 5 yr. The X-ray position is consistent with *ROSAT* source 1RXS J162535.1+632333: given the hard spectrum of this source in *XMM–Newton* and in *Swift* observations this identification is uncertain. We therefore searched for a source in RASS at the new XRT enhanced X-ray position (Table 2) which resulted in a non-detection. This source may be a variable, absorbed AGN.

A22 XMMSL1 J164859.4+800507

The XRT position, the most uncertain of this sample, coincides with the *ROSAT* source 1RXS J164843.5+800506, which could not be classified as it is reportedly blended with another source in the Hamburg/RASS data. No soft X-ray variability is detected between the XRT and RASS observations (using now the XRT position to extract a RASS flux) 16.5 yr apart. Our catalogue searches resulted in two optical sources within the error circle: a ~ 14 mag source 1 arcsec distant and a ~ 19 mag source 3.4 arcsec distant. This source is clearly associated with the 20 cm radio source NVSS 164843+800516. While a Galactic origin is not ruled out, this source is more likely to be extragalactic in nature.

A23 XMMSL1 J175542.2+624903

This source was observed twice by both with *Swift* and *XMM–Newton* and shows X-ray variability. This source is coincident with 1RXS J175546.2+624927 discovered by *ROSAT*. It is listed in the Large Quasar Astrometric Catalogue (Souchay et al. 2009) as being at redshift $z = 0.236$, and the same source is recorded in the optical identification of *ROSAT*-FSC sources (Mickaelian et al. 2006), *ROSAT* NEP X-ray source catalogue (Henry et al. 2006) and *ROSAT* North Ecliptic Pole Survey (Gioia et al. 2003) classed as type 1 AGN. The RASS flux at the XRT position is a factor of 2 lower than during the XRT observation. The source type indicators presented in this paper are consistent with this classification.

A24 XMMSL1 J182707.5−465626

Comparison with *XMM–Newton* flux and *ROSAT* flux limits shows this to be a strongly X-ray variable source. It is among the most variable of the detected sample when compared with *XMM–Newton* observations, decreasing by a factor of 11. From the X-ray to optical flux ratio and nIR colours this source could be an AGN, which would contradict the proper motion measurement of the optical counterpart.

A25 XMMSL1 J185314.2−363057

The X-ray to optical flux ratio places this source at the border between traditional AGN and low luminosity or less active galaxies however the optical counterpart displays proper motion and its nIR colours are typical of a main-sequence star of type M, strongly suggesting this source is Galactic.

A26 XMMSL1 J185608.5−430320

This source is detected with *Swift* BAT, with the highest significance (4σ) among the BAT-detected sources in this sample. One nIR counterpart is present within 15 arcsec of the *XMM–Newton* Slew Survey position with $J \leq 14$.

A27 XMMSL1 J211420.7+252419

We extracted the X-ray flux seen by RASS at the new XRT enhanced X-ray position (Table 2) using the spectral shape measured by XRT (Table 4) and recover a detection. No variability is detected between the XRT and RASS observations 16.2 yr apart while the flux decreased by a factor of ~ 4 in the 3 yr between the *XMM–Newton* and XRT observations.

A28 XMMSL1 J215905.6−201604

No single optical/nIR match was found in catalogue searches: two optical sources lie within the XRT error circle, both at 14–15 mag. One lies 0.8 arcsec from the XRT position and has a measured proper motion, while the other lies at 3 arcsec with no PM measurement. X-ray variability is apparent: during the *Swift* observation the flux was (3 ± 2) per cent of that observed with *XMM–Newton* and ≤ 20 per cent of that observed with *ROSAT*. A deeper investigation is needed to reveal the nature of this source.

This paper has been typeset from a TeX/LaTeX file prepared by the author.